Sr Isotopes in Western Aleutian Seafloor Lavas: Implications for the Source of Fluids and Trace Element Character of Arc Volcanic Rocks

Gene M. Yogodzinski [a] gyogodzin@geol.sc.edu
Peter B. Kelemen [b] peterk@ldeo.columbia.edu
Kaj Hoernle [c] khoernle@geomar.de
Shaun T. Brown [a,d] stbrown@lbl.gov
Ilya Bindeman [e] bindeman@uoregon.edu
Jeffrey D. Vervoort [f] vervoort@wsu.edu
Kenneth W.W. Sims [g] ksims7@uwyo.edu
Maxim Portnyagin [c, h] mportnyagin@geomar.de
Reinhard Werner [c] rwerner@geomar.de

a Department of Earth & Ocean Sciences, University of South Carolina, 701 Sumter St., EWSC617, Columbia, South Carolina, 29208 USA

b Lamont-Doherty Earth Observatory, Earth Institute at Columbia University, 61 Route 9W, Palisades, New York, 10964 USA

c GEOMAR - Helmholtz Centre for Ocean Research, Kiel Wischhofstrasse 1-3, D-24148 Kiel, Germany

d Energy Geosciences Division, E.O. Lawrence Berkeley National Laboratory, 1 Cyclotron Rd MS 70A-4418, Berkeley, California, 94720 USA

e Department of Geological Sciences, University of Oregon, 1275 East 13th Avenue, Eugene OR 97403-1272

f School of Earth & Environmental Sciences, Washington State University, P.O. Box 642812 Pullman, Washington, 99164-6376 USA

g Department of Geology & Geophysics, University of Wyoming, 1000 East University Avenue, Laramie, WY 82071-2000 USA

h V.I. Vernadsky Institute of Geochemistry and Analytical Chemistry, Kosigin st. 19, 119991 Moscow, Russia

Abstract

High Mg# andesites and dacites (Mg# = molar Mg/Mg+Fe) from western Aleutian seafloor volcanoes carry high concentrations of Sr (often >1000 ppm) that is unradiogenic ($^{87}Sr/^{86}Sr <$ 0.7029) compared to lavas from emergent volcanoes throughout the arc (200-800 ppm Sr, $^{87}Sr/^{86}Sr > 0.7030$). Data patterns in plots of $^{87}Sr/^{86}Sr$ vs Y/Sr and Nd/Sr imply the existence of an eclogite-melt source component – formed by partial melting of MORB eclogite in the subducting Pacific Plate — which is most clearly expressed in the compositions of western Aleutian andesites and dacites (Nd/Sr and Y/Sr <0.02) and which dominates the source budget for Sr in volcanic rocks throughout the arc. When viewed in combination with inversely correlated ϵ_{Nd} and $^{87}Sr/^{86}Sr$, these patterns rule out aqueous fluids as a dominant source of Sr because mixtures of fluids from altered oceanic crust with depleted mantle and sediment produce compositions with $^{87}Sr/^{86}Sr$ higher than in common Aleutian rocks. The unradiogenic nature of Sr in the western Aleutian andesite-dacite end-member may be understood if H_2O required to drive melting of the subducting oceanic crust is transported in fluids containing little Sr. Mass balance demonstrates that such fluids may be produced by dewatering of serpentinite in the mantle section of the subducting plate. If the eclogite-melt source component is present throughout the Aleutian arc, melting of the subducting plate must extend into minimally altered parts of the sheeted dike section or upper gabbros, at depths >2 km below the paleo-seafloor. Oxygen isotopes in western Aleutian seafloor lavas, which fall within a narrow range of MORB-like values ($\delta^{18}O$=5.1-5.7), are also consistent with this model. These results indicate that the subducting Pacific lithosphere beneath the Aleutian arc may by significantly hotter than is indicated my most thermal models.

1. Introduction

The source of island-arc magmas is widely viewed as a mixture of upper mantle and recycled components derived from seawater, subducted basalt and marine sediment. The element Sr provides unique constraints on subduction magma source models, because it is a fluid-mobile element that is both abundant and relatively unradiogenic in arc rocks. This is particularly clear in the Aleutians, where basalts commonly have 400-500 ppm Sr and Sr/Nd of 30-50, indicating 3-times higher Sr/Nd than similarly evolved MORB (~5-10% MgO), which typically have 85-150 ppm Sr and Sr/Nd = 5-20. Despite these strong enrichments, Aleutian basalts have $^{87}Sr/^{86}Sr$ that is offset from MORB only slightly (median Aleutian $^{87}Sr/^{86}Sr$ ~0.7032 versus ~0.7028 in global MORB). Hawkesworth et al. (1993) and others have noted that arc volcanic rocks globally with high Sr abundances commonly carry relatively unradiogenic $^{87}Sr/^{86}Sr$. These patterns imply that there is an abundant source of unradiogenic Sr in arc volcanic rocks, which is not present in MORB. This source is generally inferred to be from a subducted/recycled source (e.g., Hawkesworth et al., 1979; Kay, 1980). This presents a puzzle because abundant sources of subducted Sr lie predominantly in sediment (GLOSS $^{87}Sr/^{86}Sr$ = 0.712 to 0.717) and altered oceanic crust (AOC $^{87}Sr/^{86}Sr$ ~ 0.705, Staudigel, 2003 and references therein), both of which are more radiogenic than average island arc basalt ($^{87}Sr/^{86}Sr$ ~ 0.7034, Hawkesworth et al., 1991).

In this paper, we explore the implications of seafloor lavas from the western Aleutian arc with respect to the source of Sr and geochemically related trace elements. We focus on high-Sr (adakitic) andesites and dacites from the western Aleutians, because formation of these rocks involves small degrees of fluid-saturated melting of MORB eclogite, which creates a Sr-rich, geochemical component that is present in volcanic rocks throughout the Aleutian arc (Yogodzinski et al., 2015 and references therein). New Sr and oxygen isotope data presented in this paper are consistent with previous findings which indicate that the eclogite melt source

component is a major carrier of incompatible trace elements present in Aleutian volcanic rocks (e.g., Kelemen et al., 2003b; Yogodzinski and Kelemen, 1998). Results presented here also indicate that H_2O-bearing fluids required to drive melting of the subducting oceanic crust are likely to have carried little Sr and may have been produced by dehydration of serpentinite in the mantle section of the subducting lithosphere.

2. Samples, Data, and Background

The western Aleutian seafloor lavas were collected by dredging from the Ingenstrem Depression and Western Cones areas (Fig. 1) with the U.S. *R/V Thompson* during Western Aleutian Volcano Expedition in 2005 (The WAVE), and with the German *R/V Sonne*, during KALMAR and BERING cruises in 2009 and 2016 (SO201-1b, SO249-1). Here, we refer to the Ingenstrem and Western Cones samples collectively as the *western Aleutian seafloor lavas*. In this paper we present new, whole-rock Sr isotope ratio measurements on 54 samples as well as 32 oxygen and 10 hydrogen isotope measurements on mineral separates from 12 samples.

Western Aleutian lavas define a highly calc-alkaline igneous series from 50 to 70% SiO_2 in which most rocks have Mg# >0.60 (Fig. 2a). If such a series was created by fractional crystallization, hydrous and likely oxidizing conditions during basalt formation and evolution would be required (e.g., Sisson and Grove, 1993). In fact, petrographic observations indicate that pre-eruptive H_2O contents were high (Yogodzinski et al., 2015). However, because isotopic compositions change systematically toward more depleted compositions with increasing SiO_2 the western Aleutian series cannot be interpreted as primarily the product of fractional crystallization. The series has instead, been interpreted as the product of the interaction between hydrous and silicic partial melts of subducting MORB eclogite with hotter peridotite and basalt in the overlying mantle wedge (Yogodzinski et al., 2015 and references therein). A brief review of key aspects of this and alternative interpretations is provided here.

115 The key rocks in the western Aleutian series are the high-silica dacites (rhyodacites)
116 which have ~69% SiO_2, ~2% MgO, Mg#>0.60 and highly fractionated trace element patterns
117 with Sr>1000 ppm and low abundance of heavy REEs (rare earth elements) requiring a role for
118 residual garnet. These characteristics are nothing like what we find in rhyolites of the Izu-Bonin
119 arc, or in Icelandic rhyolites or other forms of high-silica ocean-ridge volcanism, which may form
120 either by extensive fractional crystallization or by partial melting of mafic crust (e.g., Lacasse et
121 al., 2007; Tamura et al., 2009; Wanless et al., 2010).
122 Melting at the base of a mafic crust is a viable model for creating high-silica magmas in
123 some arcs, but this model fails in the western Aleutians because the volcanoes that produce the
124 rhyodacites are constructed on oceanic crust of the Bering Sea, which is unlikely to be more
125 than 10 km thick. This is important because residual garnet is required in the interpretation of
126 the geochemistry, but the physical conditions that stabilize garnet during melting reactions will
127 not be realized at such shallow depths (see Yogodzinski et al., 2015 for citations and additional
128 discussion). The need for residual garnet derives from strong fractionation of the middle/heavy
129 parts of the REE pattern, resulting in high Gd/Yb (Fig. 8b in Yogodzinski et al., 2015). The
130 distinctive shape of the REE patterns in the rhyodacites likely reflects the LREE-depleted
131 pattern in the source rock (MORB), which has been rotated clockwise from the effects of
132 residual garnet. This results in low abundances of heavy REEs, enrichment in the light REEs,
133 and a flattening at both ends to create a sigmoidal shape in the REE pattern, as described by
134 O'Neill (2016) but without a role for residual amphibole.
135 More broadly, the western Aleutians is an unlikely place to produce high-silica rocks by
136 melting of the crust, because low magmatic output of the subduction zone fails to provide a
137 viable source of heat to drive melting, as seen in other parts of the Alaska-Aleutian system (e.g.,
138 Hildreth and Fierstein, 2000). In contrast, an interpretation that involves melting of the
139 subducting plate is clearly linked to a tectonic setting of oblique convergence in the western

Aleutians which produces a relatively hot subducting plate (Yogodzinski et al., 1995; 1994) as well as a cool and perhaps stagnant mantle wedge compared to the central and eastern Aleutians, where advection of hot peridotite into the wedge corner is driven by higher subduction rates (Kelemen et al., 2003b; Yogodzinski et al., 2015). Thus, the combined geologic setting and geochemical data favor models that involve melting of MORB eclogite of the subducting plate and appear to leave no viable alternatives (Yogodzinski et al., 2015 and references therein).

3. Analytical Methods

Strontium isotope ratios reported here were determined in laboratories at Washington State University, the Woods Hole Oceanographic Institution, and the University of South Carolina. All results are corrected to an $^{87}Sr/^{86}Sr$ value of 0.710240 for the NBS987 Sr isotope standard. Analytical procedures used in these laboratories and external precision based on repeat analyses of standards are summarized below. References to publications containing additional analytical information are also provided.

At South Carolina, rock powders used for Sr isotope analyses were leached with 6 M HCl in Teflon capsules at ~120° C for one hour. The leached samples were digested in 4 mL of an HF:HNO_3 mixture (3:1). The samples were dried and re-dissolved in ~ 5 ml of 6 M HCl and then heated at ~95° C to incipient dryness to remove precipitates. Samples were then dissolved in 2.5 N HCl and centrifuged for 10 minutes at 40,000 rpm. The centrifuged samples were loaded onto a ~5 mL bed of cation-exchange resin (200-400 μm Eichrom 50W-X8) in Teflon columns. The Sr fraction was separated from the rock matrix by elution in 2.5 N HCl. Strontium fractions were dried, dissolved in 0.001 N HNO_3 and loaded on an Eichrom SR-B50-S resin in Teflon micro-columns. The samples were rinsed with 3.5 N HNO_3 and separated from the resin with

0.001 N HNO_3. Isotope ratios were measured on the Thermo Fisher Neptune in the Center for Elemental Mass Spectrometry. Results were normalized to $^{86}Sr/^{88}Sr=0.1194$.

At Washington State, samples were prepared from aliquots of whole-rock powders and were dissolved at high pressure in steel-jacketed Teflon bombs in a 10:1 mixture of concentrated Hf and HNO_3 at 150° C for 5-7 days. Samples were initially separated on cation exchange columns using AG 50W-X8 resin (200-400 mesh) and were purified using micro-columns (0.18 ml rein volume) with Sr-spec resin and HNO_3. Analyses were made using a Thermo-Finnigan Neptune multicollector (MC)-ICP-MS system. Results were corrected for mass fractionation using $^{86}Sr/^{88}Sr = 0.1194$ and normalized to NBS-987. Uncertainties listed in Table 1 reflect in-run error only, presented as two standard errors.

At WHOI, samples prepared for Sr isotopes were prepared according to the details outlined in the supplemental information of Sims et al., 2013. Rock powders were leached for ~1 hour in hot 6.2 M HCl, and then rinsed repeatedly with 18MΩ H_2O. Leached powders were dissolved in a concentrated HF:$HClO_4$ mixture, followed by conversion of fluorides to chlorides by drying down three times with 6.2 N HCl. Strontium separation was done by conventional ion-exchange chromatography using DOWEX 50 cation-exchange resin. The total procedural blank for Sr was <400 pg. All Sr isotopes were measured at WHOI by MC-ICPMS using the ThermoFinnigan NEPTUNE. Strontium isotopic ratios were normalized for instrumental mass fractionation relative to $^{86}Sr/^{88}Sr = 0.1194$ also using an exponential law. For Sr isotopic measurements, the internal precision was 5–10 ppm (2σ). The external precision, after adjusting to 0.710240 for the NBS987 Sr standard was <30 ppm (2σ) for Sr.

Oxygen isotope analyses were performed by laser fluoridation using a 35 W New Wave laser on one or two mineral grains (1.2-1.5 mg) using purified BrF_5 as a reactant. Generated gases were passed through a series of cryogenic traps cooled by liquid nitrogen, and a hot Hg diffusion pump to strip away excess F_2 gas resulting from disproportionation of the reagent upon

lasing. Oxygen (O_2) was converted to CO_2 using a small Pt-C converter and yields of generated gas were measured. Analyses were run on a MAT253 gas source mass spectrometer connected to the laser fluorination-vacuum line. The San Carlos olivine ($\delta^{18}O$ = 5.25‰) and Gore Mountain garnet ($\delta^{18}O$ = 5.75‰) standards were run to calibrate day-to-day variation and to normalize the data to the SMOW scale with an offset 0.0‰. The uncertainty in the $\delta^{18}O$ measurement is 0.10 ‰ based on repeat analyses of standards run with unknowns. For hydrogen isotopes of amphibole separates, we used a glassy carbon TC/EA continuous flow system at 1450°C integrated by helium flow to the MAT253 mass spectrometer. Analytical standards (USGS57, USGS58, NBS30) were run concurrently with the unknowns. Values for δD are calibrated relative to SMOW using the USGS57 and USGS58 mica standards. Uncertainties on the standards were ±1.5‰ δD and 0.11 wt% H_2O. Additional details about the method may be found in Bindeman et al. (2012).

4. Results

Strontium isotope compositions of western Aleutian seafloor lavas (Table 1) change systematically with SiO_2. Basalts have $^{87}Sr/^{86}Sr$ ~0.70315, which is a typical for basalts throughout the arc. At higher silica the trend is toward less radiogenic Sr. Dacites with SiO_2>0.67% are the least radiogenic with $^{87}Sr/^{86}Sr$ from 0.70259 to 0.70263 (Fig. 2b). These are among the lowest Sr isotope ratios observed in arc magmas, and they are coupled with the some of the highest Nd and lowest Pb isotope ratios in arc lavas worldwide (Kelemen et al., 2003a; Yogodzinski et al., 2015). Most western Aleutian seafloor lavas have high Sr (>800 ppm) at intermediate and high-silica contents (Fig. 2c) and show progressively lower $^{87}Sr/^{86}Sr$ with increasing SiO_2 (Fig. 2b). Like Sr, Pb and Nd isotope ratios also become more depleted with increasing SiO_2 from basalt to dacite (Yogodzinski et al., 2015). Strontium isotopes show an inverse correlation with Sr abundance, similar to the correlation between Sr isotopes and SiO_2

(Fig. 3a). Thus, low-Sr basalts have high Sr isotope ratios, while andesites and dacites with higher Sr concentrations have lower $^{87}Sr/^{86}Sr$ (Fig. 2). Other Aleutian lavas with similarly unradiogenic Sr are observed at Piip Volcano, which is a highly calc-alkaline center on the seafloor north of the Komandorsky Islands (Fig. 1). Samples from Piip include many high-Mg# andesites and dacites with low $^{87}Sr/^{86}Sr$ (<0.7028) but moderate Sr abundances (300-500 ppm) similar basalts and andesites throughout the Aleutians (Fig. 3a).

In Nd-Sr isotope space, western Aleutian dacites with the least radiogenic Sr also have the most radiogenic Nd (ε_{Nd} up to +10.0). However, the dominant pattern for the western Aleutian samples is a flat trend, with ε_{Nd} falling mostly between +8.5 and +9.5 over a relatively wide range of Sr isotopes (Fig. 4a). This is particularly evident when the trend for the western seafloor lavas is compared to the whole Aleutian data field, which shows a strong inverse relationship for Nd and Sr isotopes (Fig. 4a). A similar pattern emerges for Pb isotopes, which are well correlated with $^{87}Sr/^{86}Sr$ but form a pattern that is slightly less steep than the main Aleutian array (Fig. 4b).

Oxygen isotopes were measured on mineral separates (primarily olivine and amphibole) from 12 western Aleutian samples (Table 2). Amphibole analyses were adjusted downward by 0.4 ‰ to create olivine-equivalent compositions ($\delta^{18}O_{olivine}$) at 1000° C (Bindeman et al., 2005). These values are plotted in Fig. 5. Of 29 measurements on olivine and amphibole, 21 have $\delta^{18}O_{olivine}$ between 5.0 and 5.3, and so fall within the compositional range of MORB (Cooper et al., 2009). These include a mixture of olivine separates from basalts and amphibole separates from andesites and dacites. The remaining 7 olivine and amphibole analyses have $\delta^{18}O$ from +5.4 to + 5.7 (Table 2). The oxygen isotope data show no systematic change across widely variable whole-rock compositions for SiO_2, $^{87}Sr/^{86}Sr$, La/Yb or Sr/Y (Fig. 5).

Separates of other minerals from sample TN182-07-002 (Table 2) produced variable results with relatively high $\delta^{18}O$ in quartz (+9.5) and plagioclase (+7.0), but low $\delta^{18}O$ (+4.6) in

239 clinopyroxene (Table 2). These variable $\delta^{18}O$ results and the presence of quartz xenocrysts
240 indicate that sample TN182-07-002 is a hybrid or mixed rock that likely assimilated altered
241 oceanic crust at shallow depths. Despite its complicated and apparently contaminated nature,
242 olivine and amphibole separates from this sample fall within a narrow range ($\delta^{18}O_{olivine}$ = +5.2 to
243 +5.4) and are similar to olivine and amphibole from all other samples (Fig. 5). The origins of
244 these MORB-like oxygen isotope compositions, which reflect the dominant source of the rocks,
245 are discussed further below.
246 Hydrogen isotopes in amphibole separates (Table 2) encompass the nominal mantle
247 range of -40 to -80 ‰ (Taylor and Sheppard, 1986) when correcting for ~15‰ amphibole-melt
248 fractionation (Tollan et al., 2012). Values for δD are generally higher in samples with higher
249 amphibole H_2O (Table 2), but are not correlated with whole-rock isotope or trace element
250 parameters.
251
252 **5.0 Discussion**
253 **5.1 Expression of the Eclogite Melt Source Component via Sr and $^{87}Sr/^{86}Sr$**
254 We previously emphasized that high-Sr andesites and dacites among the western
255 Aleutian seafloor lavas have characteristics expected in a geochemical source component
256 produced by partial melting of MORB eclogite in the subducting oceanic crust (Yogodzinski et
257 al., 2015). We also showed that this source component appears to be present in volcanic rocks
258 throughout the Aleutian arc. In this context, an important aspect of these rocks, which has not
259 been discussed, is the unradiogenic nature of their Sr and their high Sr abundances relative to
260 other trace elements in comparisons to common Aleutian lavas and MORB.
261 In partial melts of MORB eclogite, Sr will fractionate from Ta, Nb, Y and heavy rare-earth
262 elements (REEs), which partition into residual garnet and rutile. The incompatible behavior of
263 Sr and relatively high abundance of Sr in MORB compared to mantle peridotite, also leads to

the formation of Sr-rich magmas (Kay, 1978). As a result, plots of $^{87}Sr/^{86}Sr$ against Sr abundance, La/Ta, La/Yb, or Hf/Lu (Fig. 4) show strong inverse relationships for western seafloor lavas and in some cases, for all Aleutian volcanic rocks.

When all Aleutian data are considered, including samples from Piip Volcano, which are consistently offset toward mantle compositions in most plots of this type (Yogodzinski et al., 2015), the resulting data patterns (Fig. 4) are triangular in shape, with corners pointing toward subducted sediment and altered oceanic crust (upper-left), depleted mantle (lower-left) and eclogite melt (lower-right). Data patterns in these plots illustrate the point made in the introduction, that fluids and melts from altered oceanic crust and sediment cannot be the dominant source for Sr in Aleutian rocks. This point is most clearly illustrated in graphs of $^{87}Sr/^{86}Sr$ vs Y/Sr and Nd/Sr, where mixing lines are straight and plotted on an expanded scale to show sediment compositions at high $^{87}Sr/^{86}Sr$ (Figs. 6-7). It is evident from these plots that mixing of components from the depleted mantle, sediment and altered oceanic crust will generally produce compositions with $^{87}Sr/^{86}Sr$ greater than most Aleutian rocks. The patterns are unchanged if ratios with other light REEs are used on the horizontal scale (La/Sr, Ce/Sr, etc.). It is evident from these relationships that the Sr-rich and unradiogenic end-member in the Aleutian source must have Nd/Sr ~ 0.01 and $^{86}Sr/^{86}Sr$ <0.7029. These are characteristics of the eclogite melt source component as expressed in high-Sr andesites and dacites from the western Aleutians. They are not the characteristics of fluids from altered oceanic crust (Figs. 6-7), which will commonly have $^{87}Sr/^{86}Sr$ from 0.7035 to 0.7050 (Staudigel, 2003 and refrences therein).

A better trace element proxy for subduction fluids may be Ba/Th (George et al., 2003; Hawkesworth et al., 1997; Turner et al., 1996). However, Ba/Th has a narrow range in Aleutian rocks, from approximately 100 to 300 (Fig. 8). High concentrations of both elements appear to be linked to subducted sediment, so ratios such as Ba/La and Th/La are correlated with Pb and Sr isotopes and inversely correlated with ε_{Nd} (Kay and Kay, 1994; Kelemen et al., 2003b;

289 Yogodzinski et al., 1994). As is the case in the Aleutians, Ba and Th concentrations are
290 positively correlated in arc lavas worldwide (Fig. 12 in Kelemen et al., 2003a). Lavas with high
291 Ba/Th have very low Ba and Th concentrations, whereas those with low Ba/Th have high
292 concentrations of both elements. These important details are obscured by the use of element
293 ratios only.

294 In a plot of $^{87}Sr/^{86}$ versus Ba/Th (Fig. 8), Aleutian lavas fall along binary mixing lines
295 between MORB or depleted mantle and sediment. Thus, the $^{87}Sr/^{86}Sr$ versus Ba/Th plot fails to
296 separate the eclogite melt and depleted mantle components and so cannot be used to quantify
297 source characteristics. Something the $^{87}Sr/^{86}Sr$ versus Ba/Th plot does illustrate is that mixtures
298 of depleted mantle with fluids from altered oceanic crust will generally have Ba/Th higher than
299 Aleutian lavas (Fig. 8). Our main conclusion is that although some Ba/Th enrichment in Aleutian
300 volcanic rocks from fluids derived from seawater-altered oceanic crust cannot be ruled out, the
301 observed, correlated enrichments in both Ba and Th in Aleutian rocks must come predominantly
302 from a subducted sediment component (Kay and Kay, 1994; Kelemen et al., 2003b; Plank,
303 2005; Yogodzinski et al., 1994).

304 The strong inverse correlation between Nd and Sr isotope ratios observed in Aleutian
305 volcanic rocks (Fig. 9) reinforces the point that subducted sediment contributes significant Sr
306 and Nd to the Aleutian source (Class et al., 2000; Kay, 1980; Plank, 2005), and that the
307 dominant mixing is between sediment and one or more depleted end-member(s) with $^{87}Sr/^{86}Sr <$
308 0.703. Again, in Fig. 9 as in many isotope-isotope plots, we infer that there must be two source
309 components at the depleted end of the mixing array (Yogodzinski et al., 2015). One is the
310 eclogite melt component, which has high Sr/Nd and produces strongly curved mixing lines with
311 sediment. The other is the depleted mantle, which has Sr/Nd similar to bulk sediment, and so
312 produce straight mixing lines. The two end-member mixing lines encompass the data field for
313 Aleutian volcanic rocks (Fig. 9).

Thus, the combined data patterns in Figs. 8 -10 indicate that aqueous fluids from altered oceanic crust cannot be a dominant contributor of Sr to the source of Aleutian volcanic rocks. These results also imply that in Aleutian rocks, the dominant source of unradiogenic subducted Sr may be produced by melting of MORB eclogite in the subducting plate (i.e., it is the eclogite-melt source component - Yogodzinski et al., 2015). Moreover, the combination of high Sr and unradiogenic Sr isotopes is observed in arc volcanic rocks globally (Hawkesworth et al., 1993).

Basic modeling results indicate that much of the fractionation of Sr from Nd concentrations observed in high-Sr, western Aleutian dacites (Nd/Sr~0.01) compared to MORB (Nd/Sr~0.09) is produced by residual garnet. Using bulk solid/liquid partition coefficients from the Kessel et al. (2005) experiments at 900° C and 4 GPa (D_{Sr}=0.047, D_{Nd}=0.662), a 5% batch melt of Pacific MORB with Sr~128 ppm and Nd/Sr ~ 0.095 (Gale et al., 2013), will have 1347 ppm Sr and Nd/Sr of 0.013. Kessel et al. (2005) report that garnets in this experiment had Nd/Sr = 69.6 (Nd = 41± 6 ppm, Sr = 0.60 ± 0.2 ppm) and so likely account for most of the fractionation of Nd/Sr from ~0.09 in the MORB eclogite source to ~0.01 in the eclogite melt. Partitioning from experiments at 1000° C and 4 GPa (Kessel et al., 2005) produce eclogite melts with similar Sr abundances and slightly higher Nd/Sr (Sr = 1371 ppm, Nd/Sr=0.026). Thus, fluids from altered oceanic crust and melts of MORB eclogite produce similar fractionation of Sr from Nd (Fig. 7), but not Ba from Th (Fig. 8). More broadly, the decoupling of Ba and Sr enrichments from Nd (Fig. 10) indicates that aqueous fluid enrichment is not a significant factor in controlling Ba and Sr budgets in Aleutian rocks (see also figure 12 in Kelemen et al., 2003a). Again, enrichments in Ba are linked primarily to a subducted sediment in Aleutian rocks (Fig. 8) and appear unrelated to enrichments in Sr which are linked to the eclogite melt component and appear to be controlled by residual garnet (Fig. 10).

339 **5.2 Subducted Serpentinite as a Source of H_2O and Sr**

340 The unradiogenic nature of Sr in western Aleutian andesite and dacite ($^{87}Sr/^{86}Sr<0.7027$)
341 is perhaps surprising, given our interpretation that these lavas contain a substantial component
342 derived by hydrous partial melting of subducted basalt, which should carry relatively radiogenic
343 Sr, due to effects of seawater alteration. This is an acute problem for the end-member western
344 Aleutian samples, because their Sr concentrations are high (Sr>1000 ppm) and because
345 petrographic observations indicate that they are H_2O-rich (Yogodzinski et al., 2015).

346 Fluids held in micas and amphiboles and other hydrous minerals in seawater-altered
347 MORB could drive in-situ, fluid-absent melting within subducting oceanic crust (e.g., Beard and
348 Lofgren, 1991). However, H_2O in hydrous minerals in such a source was derived from seawater,
349 and will commonly contain radiogenic Sr with $^{87}Sr/^{86}Sr$ ~0.704 (Staudigel, 2003). Fluid-absent
350 melting of such a source cannot contribute significantly to the formation of western Aleutian
351 high-Sr dacites, which have $^{87}Sr/^{86}Sr$~0.7026 (Fig. 3a). Assuming that potential sources of H_2O
352 lie primarily in subducting sediment and AOC (which contain radiogenic Sr), it is evident from
353 the unradiogenic nature of Sr in western Aleutian andesites and dacites that the H_2O they
354 contain cannot have been transported in fluids that contributed significantly to their Sr budgets.

355 One source of H_2O with low Sr is partially serpentinized peridotite within the mantle
356 section of the subducting plate, which may be formed in ocean ridge hydrothermal systems and
357 by seawater ingress along normal faults formed as the subducting plate passes over the outer
358 rise and descends into the trench (Peacock, 2001; Ranero et al., 2003). Serpentine formed in
359 the cool interior of the subducting plate may be transported to its maximum pressure stability of
360 ~7 GPa, which extends beyond subarc depths (Ulmer and Trommsdorff, 1995). As the
361 subducting plate descends, an inverted geothermal gradient of >200-300° C is established, so
362 the top of the plate may be heated to temperatures required for fluid-saturated melting (700-
363 750° C at 3 GPa), at approximately the point where serpentinite dehydration creates fluid

364 release from the plate's interior. This creates a situation where melting of basaltic crust within
365 the subducting plate can be fluxed by fluids produced by dehydration of the underlying
366 serpentine (Poli and Schmidt, 2002; Portnyagin et al., 2007; Walowski et al., 2015).
367 Partially serpentinized mantle peridotites have a range of Sr concentration and $^{87}Sr/^{86}Sr$,
368 depending on water/rock ratios in the systems that lead to serpentinization. We assume the
369 worst case for our purposes, which is that Sr carried in fluids from dewatered serpentinite
370 beneath the Aleutian arc has the isotopic composition of modern seawater ($^{87}Sr/^{86}Sr = 0.709$).
371 With this starting point, the two things needed to calculate a mass balance for the source of
372 Aleutian Sr are (1) the Sr abundance in the serpentinite that is the source of the fluid and (2) the
373 Sr abundance in the aqueous fluid produced by dehydration of that serpentinite.
374 Serpentinized abyssal peridotites are formed predominantly by the interaction of
375 seawater with depleted peridotite and so provide a reasonable estimate for serpentinite formed
376 within the subducting plate and entering the Aleutian subduction zone. In data for 84 abyssal
377 peridotites compiled by Deschamps et al. (2013), the average Sr abundance is aliased by 9
378 samples with >100 ppm Sr, including three with >1000 ppm Sr. Of the remaining 75 analyses,
379 72 contain <10 ppm Sr. If the 9 anomalous samples are excluded, the mean Sr abundance in
380 the filtered dataset is 3.5 ppm ± 6.3 (1σ). Based on these values, it is reasonable to infer that
381 serpentinite within the subducting plate as it enters the Aleutian subduction zone will not
382 generally contain more than ~16 ppm Sr (the average plus two standard deviations).
383 Experimental studies provide a basis for estimating Sr abundances in fluids produced by
384 dehydration of serpentinite. Tatsumi et al. (1986) found that 10 to 19% of Sr was extracted from
385 serpentinite during dehydration, which was measurably less than the 17-25% extraction of La.
386 Tenthorey and Hermann (2004) found that fluids produced by serpentine dehydration in
387 diamond trap experiments never had higher Sr than their starting material, and in this respect,
388 their results for Sr were similar to those for Ce. Concentrations of Sr in fluids derived by

389 serpentine dehydration at 3.5 GPa were 1.6 to 1.8 – times higher than in the starting
390 serpentinite composition (Spandler et al., 2014) similar to fluid/rock partitioning of Ce (3.0-3.8)
391 and less than for Cs (10-16) and Pb (8.6-9.4). Thus, experimental results indicate that Sr
392 concentrations in fluids produced by dehydrating serpentinite will not be more than a factor of ~2
393 greater than Sr concentrations in the source. Fluids produced by dehydration of serpentinized
394 peridotite with less than 16 ppm Sr should contain no more than 32 ppm Sr. This estimate is
395 similar to Sr abundances of 20-30 ppm measured in fluid inclusions in olivine-orthopyroxene-
396 chlorite rocks produced by prograde metamorphism of serpentinite at subduction depths
397 (Scambelluri et al., 2004).
398 Assuming that 2% H_2O is sufficient to drive significant melting of MORB eclogite (e.g.,
399 Schmidt et al., 2004), the addition of seawater Sr in the fluid ($^{87}Sr/^{86}Sr = 0.709$) to Pacific MORB
400 eclogite ($^{87}Sr/^{86}Sr = 0.70255$) will raise $^{87}Sr/^{86}Sr$ in the mixture over fresh MORB by only 0.00003
401 to 0.00005, for 80 to 130 ppm Sr in eclogite. In other words, if Pacific MORB eclogite has 80-
402 130 ppm Sr and $^{87}Sr/^{86}Sr = 0.70255$, the addition of 2% of fluid with 32 ppm Sr and $^{87}Sr/^{86}Sr =$
403 0.709 will produce rock-fluid mixtures with $^{87}Sr/^{86}Sr$ from 70258 to 0.70260. This mass balance
404 indicates that fluids produced by dehydration of serpentinite in the mantle section of the
405 subducting Pacific Plate will carry little Sr and have minimal impact on the isotopic composition
406 of the source mixture if MORB eclogite with 80-130 ppm Sr is the dominant source of the melt.
407 This simple model provides a mechanism by which high-Sr dacites from the western
408 Aleutians, which have $^{87}Sr/^{86}Sr$ ~0.7026, may represent the end-member eclogite-melt source
409 component for Sr, as they do for Pb, Nd and Hf (Yogodzinski et al., 2015). It must also be true
410 that the source of the high-Sr dacites does not contain a significant quantity of subducted
411 sediment, and that the bulk of the MORB eclogite source in the subducting plate cannot have
412 been greatly affected by seawater alteration. These points are discussed further below. An
413 important additional result of this model is that it decouples the dominant source of H_2O, derived

414 by dehydration of subducting serpentine, from the dominant source of incompatible trace
415 elements, produced via partial melting of subducted sediment and basalt. This decoupling of
416 H_2O and trace element sources is also suggested by the observation of widely variable trace
417 element abundances compared to more restricted variability for H_2O inferred from least-
418 degassed melt inclusions in the global arc database (Plank et al., 2013; Portnyagin et al., 2007).
419
420 **5.3 Subducted Oceanic Crust as a Source of Sr**
421 The end-member character of western Aleutian andesites and dacites in many isotope-
422 trace element ratio plots (Figs. 4 and 7-11) is a reflection of their isotopically depleted
423 compositions ($^{87}Sr/^{86}Sr$ ~0.7026) combined with Sr-rich (Nd/Sr~0.01) and fractionated trace
424 element patterns. These are distinctive characteristics compared to common arc lavas but they
425 are not unique globally, or even uncommon. In fact, we see qualitatively similar shifts from
426 common arc-basalt / andesite compositions toward less radiogenic Sr and higher Sr
427 abundances in high Sr/Nd andesites and dacites in many Circum-Pacific locations, including
428 Baja California (Rogers et al., 1985), Patagonia (Stern and Killian, 1996), Solander Island, New
429 Zealand (Foley et al., 2012), the Solomon Islands (König et al., 2007), Antarctica (McCarron and
430 Smellie, 1998), the southern-most Cascade arc (Grove et al., 2002; Walowski et al., 2015) and
431 other parts of northern California (Johnson and O'Neil, 1984). In all of these locations,
432 subducting lithosphere is young (Defant and Drummond, 1990) and/or associated with a slab
433 window or oblique convergence, where plate edges may be exposed to heating by mantle flow
434 on three sides (Yogodzinski et al., 2001). Thus, it is a hot-slab setting and a distinctive
435 geochemical pattern that unites these locations. Assuming that the geochemical pattern reflects
436 a relatively large source component produced by melting of the basaltic part of the subducting
437 plate under eclogite conditions (Defant and Drummond, 1990; Kay, 1978), the observed shift
438 toward relatively unradiogenic Sr means that in the places where the effects of eclogite melting

439 are most evident, the melting process commonly encompasses a significant portion of oceanic
440 crust that was not subject to prior effects of seawater alteration.
441 Oceanic crustal sections in ophiolites commonly exhibit extensive effects of seawater
442 alteration with $^{87}Sr/^{86}Sr$ >0.704 throughout the sheeted dikes and into the upper gabbros at
443 depths of 2-3 km (e.g., Bickle and Teagle, 1992). If it were subducted, this part of an oceanic
444 crustal section could not be the source of Sr in end-member western Aleutian dacites, which
445 have $^{87}Sr/^{86}Sr$ ~0.7026 (Fig. 3a). More broadly, such extensively altered oceanic crust cannot be
446 the source of Sr in Aleutian lavas in general because mixtures of source components from
447 Aleutian sediment ($^{87}Sr/^{86}Sr$ ~0.706), seawater-altered basalt ($^{87}Sr/^{86}Sr$ >0.704), and depleted
448 Pacific mantle ($^{87}Sr/^{86}Sr$ ~0.7025), do not encompass the compositions of Aleutian lavas in
449 $^{87}Sr/^{86}Sr$ vs Nd/Sr space (Fig. 7) or in other similar plots involving Sr isotopes.
450 Ocean drilling provide samples of oceanic crust that are less extensively affected by
451 seawater alteration (Davis et al., 2003) and so provide a more plausible subducted source for
452 Aleutian Sr. At Site 504B (eastern equatorial Pacific), where drilling penetrated 1800 m into
453 oceanic basement, the average $^{87}Sr/^{86}Sr$ of all samples in the sheeted dike section is 0.7029 (Alt
454 et al., 1996; Bach et al., 2003), which is little different from fresh MORB from the Galapagos
455 Ridge (the source of oceanic lithosphere at Site 504B), which have $^{87}Sr/^{86}Sr = 0.7028 \pm 0.0002$
456 (n=93, Gale et al., 2013). Höfig et al. (2014) similarly showed at nearby Site 1256, that
457 significant seawater alteration effects on $^{87}Sr/^{86}Sr$ were concentrated in the lower volcanic
458 section and upper sheeted dikes, with most samples at lower stratigraphic positions falling
459 within or close the range of $^{87}Sr/^{86}Sr$ observed in fresh MORB at the site. Data compiled from
460 the MARK and Atlantis II Fracture Zone areas also show modest effects of seawater alteration
461 on $^{87}Sr/^{86}Sr$ at depths of 1.5 – 2.0 km into oceanic basement (Davis et al., 2003).
462 Thus, the unradiogenic nature of Sr in Aleutian rocks overall ($^{87}Sr/^{86}Sr < 0.7036$), and in
463 end-member western Aleutian samples in particular (Figs. 4 and 7-10), means that melting of

464 the subducting plate cannot be confined to the volcanic section (near the top of the plate), where
465 seawater alteration is often extensive (Alt et al., 1996; Höfig et al., 2014; Staudigel, 2003).
466 Instead, if the eclogite melt component is the dominant source of Aleutian Sr, then eclogite
467 melting beneath the Aleutian arc must extend down to minimally altered parts of the sheeted
468 dike section, more than 2 km below the paleo-seafloor in the subducting plate. An additional
469 effect may be that extensive dehydration of seawater altered basalt at the top of the slab (as
470 predicted by thermal models - Syracuse and Abers, 2006; van Keken et al., 2011) may
471 commonly remove a significant proportion of radiogenic Sr at relatively shallow depths beneath
472 the forearc and prior to eclogite melting. If so, melts produced from the upper volcanic section at
473 greater depths would contain less radiogenic Sr than expected from seawater-altered basalt
474 with $^{87}Sr/^{86}Sr > 0.7040$ (Staudigel, 2003). This could contribute to an eclogite melt component
475 with low Nd/Sr and relatively unradiogenic Sr as required by mass balance (Figs. 7-10).
476 Finally, oxygen isotope ratios in western Aleutian lavas (Fig. 5) are similar to fresh
477 MORB and mantle values (Cooper et al., 2009). These data are inconsistent with melting
478 confined to highly altered seafloor volcanic rocks, in which relatively high $^{18}O/^{16}O$ ratios are
479 observed (Alt et al., 1996; Staudigel, 2003). Based on oxygen isotope stratigraphy at Site 504B
480 (Alt et al., 1996), melting to the base of the sheeted dikes would encompass a significant
481 proportion of oceanic crust with relatively light oxygen ($\delta^{18}O < 4$ ‰) that would offset (in a mass-
482 balance sense) heavy oxygen derived from highly altered lavas, and thereby create an eclogite
483 melt component with MORB and mantle-like oxygen isotope ratios, as seen in western Aleutian
484 lavas ($\delta^{18}O = 5.1 - 5.7$, Fig. 5). This would achieve the effects of “whole-slab melting”, as
485 discussed by Bindeman et al. (2005), though it should be noted that interaction of eclogite melts
486 with mantle peridotite as they rise to the surface may also contribute to the MORB-like and
487 mantle oxygen isotopes values in western Aleutian seafloor lavas (Fig. 5).
488

489 **5.4 Reconciling Aleutian Sr with Thermal Models**

490 Melting of subducting oceanic crust will occur where sufficient water is present and when
491 temperatures exceed the fluid-saturated solidus of MORB eclogite. The presence of these
492 conditions in a subduction zone depend on the thermal structure of a subducting plate, as
493 reflected in the thermal parameter (Φ), which is the product of slab age and the orthogonal
494 subduction rate (Kirby et al., 1991). Excluding the anomalously cold Tonga slab (Φ >14,000),
495 thermal parameters vary globally from 100-400 in hot-slab systems such as the Cascades and
496 Mexico, to 6000-7000 in cold-slab systems such as the Kuriles and South Mariana arc
497 (Syracuse and Abers, 2006). The average thermal parameter for three Aleutian locations (Φ
498 =2577, 1σ=247) is above the median for all arcs (Φ =2095) but below the coolest ~30% which
499 have Φ >4000 (Syracuse and Abers, 2006). So, the Aleutians may be considered a moderate-
500 to-cool arc. At subarc depths around 100 km (3.0 to 3.5 GPa), an ensemble of thermal models
501 yield Aleutian slab-top temperatures consistently above the fluid-saturated solidus for MORB
502 eclogite at 700-800° C (Syracuse et al., 2010). In turn, these model estimates are somewhat
503 cooler than those from geochemical proxies such as Ce/H_2O, which place Aleutian slab-top
504 temperatures ~830° C (Cooper et al., 2012; Plank et al., 2009). At the bottom of the sheeted
505 dikes in the subducting plate, which will commonly lie 2 km below paleo-seafloor, temperatures
506 are expected to be significantly cooler. Modeling results for the southern Mariana arc (Φ =6350)
507 and temperature variation within the crustal sections of subducting plates globally indicate that
508 temperatures several km below the top of subducting oceanic crust beneath the Aleutian arc
509 should be more than 100° C below the temperature at the top of the subducting plate (see figure
510 2 and 4b in van Keken et al., 2011).

511 Modeling results thus indicate that in the presence of sufficient water, melting of
512 sediment and basalt at the top of the subducting oceanic plate beneath the Aleutians is
513 possible, but that – if the subducting oceanic plate is intact – melting should not extend to the

514 base of the sheeted dike section, as our analysis of geochemical data seems to require. An
515 additional point is that dehydration of sediment and seawater altered basalt at the top of the
516 subducting plate beneath the forearc (e.g., Syracuse et al., 2010; van Keken et al., 2011) is also
517 likely to limit melt production even in the hottest part of the slab. Thus, subduction zone thermal
518 models appear to be at odds with Aleutian geochemical data presented here.

519 There are several possible ways to resolve this apparent discrepancy. Subducting plates
520 may commonly be buckled and torn (Yamaoka et al., 1986), or intensely sheared and broken at
521 the plate interface and thus exposed to heating in ways that are not captured by two-
522 dimensional thermal models (e.g., Bebout and Penniston-Dorland, 2016; Penniston-Dorland et
523 al., 2015). Heating of subducting lithosphere from below may also be a greater effect than is
524 appreciated. For example, Hawley et al. (2016) observe a low-velocity seismic anomaly
525 beneath the outer rise portion of the subducting Juan de Fuca plate along the full length of the
526 Cascadia subduction zone. If this anomaly is in fact a 900 km-long cylinder of partial melt
527 (Hawley et al., 2016) it implies the advection of heat to the base of the subducting plate which
528 may effect on the thermal structure of the plate as it passes beneath the trench and forearc and
529 enters the subduction zone. It may also be that subducting sediments and altered lavas are
530 commonly transferred from the footwall into the hanging wall along imbricate thrust faults and
531 shear zones. A variety of studies have also concluded that sedimentary sections at the top of
532 subducting plates may be physically separated from the underlying basaltic oceanic crust by
533 density instabilities leading to diapirs (Behn et al., 2011; Gerya and Yuen, 2003; Kelemen et al.,
534 2003a; Marschall and Schumacher, 2012). Evidence that this process has occurred may be
535 found in the highly depleted isotopic compositions of most seafloor volcanic rocks west of Buldir
536 Island, which indicate the geochemical influence of subducted sediment there is nearly zero
537 (Kelemen et al., 2003b; Yogodzinski et al., 2015; 1994). Such depleted compositions are most
538 easily explained if the sedimentary section and perhaps the sheared and hydrated portions of

539 the uppermost volcanic section (the mélange - Marschall and Schumacher, 2012) were
540 physically separated from the top of the subducting plate. If the sedimentary section were
541 incorporated into the mantle wedge by diapirs (Behn et al., 2011; Gerya and Yuen, 2003;
542 Kelemen et al., 2003a; Marschall and Schumacher, 2012), then increasingly oblique subduction
543 along the arc and weak coupling at the top of the slab could cause the subducting plate to
544 effectively outrun the overlying column of mantle rock so that in the westernmost parts of the
545 arc, partial melts from the basaltic part of the slab would rise in a mantle wedge that had not
546 been contaminated by sediment diapirs.
547
548 **6. Conclusions**
549 Results of this study reinforce the conclusion that high Mg# andesites and dacites from
550 seafloor volcanoes in the western Aleutians exhibit trace element and isotopic characteristics
551 produced by melting of MORB eclogite in oceanic crust of the subducting Pacific Plate. Mixing
552 relationships in plots of $^{87}Sr/^{86}Sr$ versus Nd/Sr and ε_{Nd} versus $^{87}Sr/^{86}Sr$ rule out aqueous fluids
553 as a significant source for Sr in Aleutian rocks. Water required to drive eclogite melting in the
554 oceanic crust is likely produced by serpentine breakdown in the underlying mantle section of the
555 subducting plate. Fluids produced by serpentine breakdown will carry little Sr and have minimal
556 impact on $^{87}Sr/^{86}Sr$ in the source mixture. MORB-like Sr and O isotopes in end-member samples
557 indicate that eclogite melting must encompass a bulk composition that has been little-affected
558 by seawater alteration. Eclogite melting must consequently extend to depths of 2+ km into the
559 subducting plate. These findings imply that subducting lithosphere beneath the Aleutian arc is
560 significantly hotter than indicated by most thermal models.

Acknowledgements

The authors thank E Bair, C. Frisby, S. Henrick and M. Siegrist for their assistance with data collection at the University of South Carolina, and to J. Blusztajn for his assistance at Woods Hole. Thanks also to G. Hart and C. Knaack for technical help at the ICP-MS facility at Washington State University. The cooperation of SM Kay and RW Kay is gratefully acknowledged. Thanks also go to T. Murray, T. Miller, C. Nye, M. Coombs, J. Power and others at the USGS and Alaska Volcano Observatory for their support. Support for STB during manuscript preparation was provided by the Director, Office of Science, Office of Basic Energy Sciences, of the U.S. Department of Energy under Contract No. DE-AC02-05CH11231. This paper benefitted from the helpful comments of Richard Arculus, an anonymous reviewer, and editor Mike Bickle. Their time and effort are much appreciated.

Funding

This work was supported by US National Science Foundation Grants EAR-0230261 to JDV; EAR-0510671 to KWWS; EAR-1447337 to IB; EAR-0509922, EAR-0236481, OCE-0242585 and OCE-0728077 to GMY; OCE-0242233, OCE-0533226, OCE-1144759, EAR-0727013, EAR-0961359 and EAR-0742368 to PBK. This work was also supported by the German Ministry for Education and Research for R/V SONNE cruises SO201-1b and SO249-1 (BMBF; Grants 03G0201A KALMAR and 03G0249 BERING).

FIGURE CAPTIONS

Fig. 1 Map of north Pacific and Bering, showing Aleutian locations mentioned in the text. Yellow triangles mark the locations of emergent volcanoes on Aleutian islands. Red triangles indicate the locations of western Aleutian seafloor volcanoes (see also Yogodzinski et al., 2015 for more detailed maps of western Aleutian seafloor volcanic structures).

Fig. 2 Aleutian whole-rock compositions. Large, open symbols are western Aleutian seafloor lavas from Yogodzinski et al. (2015). Gray symbols are published data for samples from emergent Aleutian volcanoes collected at locations from the western tip of the Alaska Peninsula to Buldir Island (Fig. 1). These data are from the compilation of Kelemen et al. (2003b) updated to include more recently published data. (a) FeO*/MgO versus SiO_2 with right vertical axis showing Mg# calculated on a molar basis and total iron as Fe^{2+}. The black diagonal line across the plot is the calc-alkaline (CA) – tholeiitic (TH) discriminant line of Miyashiro (1974). (b) $^{87}Sr/^{86}Sr$ and (c) Sr abundance. Strontium isotope data are from Table 1. Complete major element and trace element data (except for SO249 samples) are available in Yogodzinski et al. (2015).

Fig. 3 Whole-rock $^{87}Sr/^{86}Sr$ in Aleutian volcanic rocks versus Sr (a), Hf/Lu (b), La/Ta (c) and La/Yb (d). In each panel, the trace element ratios on the horizontal axes places the eclogite-melt source component in the lower-right of the plots and depleted mantle and MORB in the lower-left. Sediment and seawater altered oceanic crust generally have $^{87}Sr/^{86}Sr>0.7038$ and so are off-scale in the upper left. Data for Piip Seamount, located in the westernmost Aleutians (Fig. 1) are from Yogodzinski et al. (1994) and include pre-Piip (Komandor Series) samples. Other data sources are the same as in Fig. 3. MORB is the average of Juan de Fuca Ridge (northeast Pacific) data ($^{87}Sr/^{86}Sr=0.7025$, La=5.75 ppm, Yb=Y, Hf=2.81, Lu=0.519, Ta=0.445, Sr=134, Y=34.3) from Gale et al. (2013). Average DMM trace elements are from Salters and Stracke (2003) with $^{87}Sr/^{86}Sr$ also reflecting Juan de Fuca MORB.

Fig. 4 Aleutian whole-rock isotopes compared with published Pacific MORB data. (a) ε_{Nd} versus $^{87}Sr/^{86}Sr$. (b) $^{207}Pb/^{204}Pb$ versus $^{87}Sr/^{86}Sr$. Data sources except Pacific MORB are the same as in Figs. 3-4. Pacific MORB data are from published sources sources.

Fig. 5 Mineral oxygen isotope ratios ($\delta^{18}O_{olivine}$) in western Aleutian seafloor lavas versus whole-rock SiO_2 (a), $^{87}Sr/^{86}Sr$ (b), La/Yb (c) and Sr/Y (d). Oxygen isotope data are from Table 2. For amphibole samples the $\delta^{18}O_{olivine}$ is the measured $\delta^{18}O$ value form Table 2 minus 0.40 ‰ to produce an approximate olivine-equivalent composition (Bindeman et al., 2005). Whole-rock $^{87}Sr/^{86}Sr$ data are from Table 1. Other data are from Yogodzinski et al. (2015).

Fig. 6 Whole-rock $^{87}Sr/^{86}Sr$ in Aleutian volcanic rocks and sediment versus Y/Sr with source-mixing characteristics. Aleutian sediments are published data. Sediment melt Y-Sr ratios are model compositions (Yogodzinski et al., 2015) calculated from Aleutian sediment and using results of sediment-melting experiments (Hermann and Rubatto, 2009; Skora and Blundy, 2010). Fluids from altered oceanic crust (AOC – blue bar) are model compositions with Y/Sr<0.02 calculated with 5-15% fluid extraction using partitioning data from experiments at 700° and 800° C and 4 GPa by Kessel et al. (2005). The fluid source rock is seawater-altered basalt (Sr=120, Y =37.3 ppm) which is an average Pacific MORB from Gale et al. (2013) adjusted for seawater alteration using enrichment factors from the Site 801 super-composite of Kelley et al. (2003). Fluid $^{87}Sr/^{86}Sr$ values from 0.7035 to 0.7050 are similar to widely reported

compositions for seawater-altered basalt (e.g., Alt et al., 1996; Staudigel, 2003). Eclogite melts (green bar) are model compositions with Y-Sr ratios <0.002 calculated as 5-10% melts with partitioning data from Kessel et al. (2005) at 900° C and 4 GPa. The eclogite melt component has $^{87}Sr/^{86}Sr$ <0.7029 as expected for Pacific MORB + modest seawater alteration as discussed in the text. MORB and DMM and other data sources are as in Fig. 3.

Fig. 7 Whole-rock $^{87}Sr/^{86}Sr$ in Aleutian volcanic rocks and sediment versus Nd/Sr with source-mixing characteristics. Fluids from altered oceanic crust (AOC – blue bar) are model compositions with 0.008<Nd/Sr<0.016 calculated with 5-15% fluid extraction using partitioning data from experiments at 700° and 800° C and 4 GPa by Kessel et al. (2005). The fluid source rock is seawater-altered basalt (Sr=120, Nd =11.3 ppm) determined as in Fig. 7. Eclogite melts (green bar) are model compositions with 0.013<Nd/Sr<0.019 calculated as 5-10% melts with partitioning data from Kessel et al. (2005) at 900° C and 4 GPa. Other data sources and modeling parameters are as in Fig. 6.

Fig. 8 Whole-rock $^{87}Sr/^{86}Sr$ in Aleutian volcanic rocks and sediment versus Ba/Th with source-mixing characteristics. Mixtures with depleted MORB mantle use values from Salters and Stracke (2003). Fluids from altered oceanic crust (AOC – blue bar) are model compositions extracted from seawater-altered basalt (Ba=24, Th =0.34 ppm) determined as in Fig. 6. Mixing end-member 'x' is a 5% fluid at 800° C with 208 ppm Ba and 0.513 ppm Th. The total range for Ba/Th in the AOC fluids is 710-2807 based on 5-15% fluid extraction. The sediment mixing end-members are turbidites from DSDP178 (Ba/Th=232, Th=4.38 ppm) and DSDP183 (Ba/Th=112, Th=6.63). Eclogite melts (green bar) are model compositions with Ba/Th calculated as 5-10% melts using partitioning data from Kessel et al. (2005) at 900° and 4 GPa. Other data sources and modeling parameters are as in Fig. 6.

Fig. 9 Whole-rock ε_{Nd} versus $^{87}Sr/^{86}Sr$ in Aleutian volcanic rocks and sediment with source-mixing characteristics. Dashed lines are mixtures with an average bulk sediment composition with Sr=235 ppm, Nd=19.0 ppm, $^{87}Sr/^{86}Sr$=0.7068, and ε_{Nd}= -0.2. The depleted mantle mixing end-member has Nd and Sr concentrations from Salters and Stracke (2003) with $^{87}Sr/^{86}Sr$=0.7025 and ε_{Nd}=11.2, similar to northeast Pacific MORB (Gale et al., 2013). The eclogite melt end-member is an average western Aleutian dacite with Sr=1470 ppm, Nd=11.5 ppm, $^{87}Sr/^{86}Sr$=0.70262 and ε_{Nd}=9.5 (Yogodzinski et al., 2015). The AOC fluid mixing end-member is a model composition with Sr=42.2 ppm and Nd=0.652 ppm, based on a 5% fluid and partitioning from 4GPa experiments at 800° C from Kessel et al. (2005). The fluid has $^{87}Sr/^{86}Sr$=0.7040 based on typical seawater-altered basalt and ε_{Nd}=11.2 like northeast Pacific MORB (Gale et al., 2013). Other data sources and modeling parameters are as in Fig. 6.

Fig. 10 Whole-rock Sr/Nd versus Ba/Nd in Aleutian volcanic rocks and sediments compared to MORB and depleted MORB mantle (DMM). Symbols and data sources are as in Figs. 2 and 9.

678 **References**

679 Alt, J.C., Teagle, D.A.H., Bach, W., Halliday, A.N., Erzinger, J., 1996. Stable and strontium
680 isotopic profiles through hydrothermally altered upper oceanic crust, Hole 504B, in: Alt,
681 J.C., Kinoshita, H., Stokking, L.B., Michael, P.J. (Eds.), Proceedings of the Ocean
682 Drilling Program, Scientific Results, Vol. 148. Ocean Drilling Program, College Station,
683 pp. 57-69.
684 Bach, W., Peucker-Ehrenbrink, B., Hart, S.R., Blusztain, J., 2003. Geochemistry of
685 hydrothermally altered oeanic crust: DDP/ODP Hole 504B - Implications for seawater-
686 crust exchange budgets and Sr- and Pb-isotopic evolution of the mantle. Geochem
687 Geophys Geosys 4.
688 Beard, J.S., Lofgren, G.E., 1991. Dehydration melting and water-saturated melting of basaltic
689 and andesitic greenstones and amphibolites at 1, 3, and 6-9 kb. J Petrol 32, 365-401.
690 Bebout, G.E., Penniston-Dorland, S.C., 2016. Fluid and mass transfer at subduction interfaces -
691 The field metramorphic record. Lithos 240-243, 228-258.
692 Behn, M.D., Kelemen, P.B., Hirth, G., Hacker, B.R., Massonne, H.J., 2011. Diapirs as the soure
693 of the sediment signature in arc lavas. Nature Geoscience 4, 641-646.
694 Bickle, M.J., Teagle, D.A.H., 1992. Strontium alteration in the Troodos ophiolite: implication for
695 fluid fluxes and geochemical transport in mid-ocean ridge hydrothermal systems. Earth
696 Planet Sc Lett 113, 219-237.
697 Bindeman, I.N., Eiler, J.M., Yogodzinski, G.M., Tatsumi, Y., Stern, C.R., Grove, T.L., Portnyagin,
698 M., Hoernle, K., Danushevsky, L.V., 2005. Oxygen isotope evidence for slab melting in
699 modern and ancient subduction zones. Earth Planet Sc Lett 235, 480-496.
700 Bindeman, I.N., Kamenetsky, V.S., Palandri, J., Vennemann, T., 2012. Hydrogen and oxygen
701 isotope behavior during variable degrees of upper mantle melting: example from the
702 basaltic glasses from Macquarie Island. Chem Geol 310-311, 126-136.
703 Class, C., Miller, D.M., Goldstein, S.L., Langmuir, C.H., 2000. Distinguishing melt and fluid
704 subduction components in Umnak Volcanics, Aleutian Arc. Geochemistry, Geophysics,
705 Geosystems.
706 Cooper, K.M., Eiler, J.M., Sims, K.W.W., Langmuir, C.H., 2009. Distribution of recycled crust
707 within the upper mantle: Inights from the oxygen isotope composition of MORB from the
708 Australian-Antartcitc Discordance. Geochem Geophys Geosys 10.
709 Cooper, L.B., Ruscitto, D.M., Plank, T., Wallace, P.J., Syracuse, E.M., Manning, C.E., 2012.
710 Global variations in H_2O/Ce: 1. Slab surface temperatures beneath volcanic arcs.
711 Geochem Geophys Geosys 13.
712 Davis, A.C., Bickle, M.J., Teagle, D.A.H., 2003. Imbalance in the oceanic strontium budget.
713 Earth Planet Sc Lett 211, 173-187.
714 Defant, M.J., Drummond, M.S., 1990. Derivation of some modern arc magmas by melting of
715 young subducted lithosphere. Nature 347, 662-665.
716 Deschamps, F., Godard, M., Guillot, S., Hattori, K., 2013. Geochemistry of subduction zone
717 serpentinites: A review. Lithos 178, 96-127.
718 Foley, F.V., Pearson, N.J., Rushmer, T., Turner, S., Adam, J., 2012. Magmatic evolution and
719 magma mixing of Quaternary adakites at Solander and Little Solander Islands, New
720 Zealand. Journal of Petology 54, 703-744.
721 Gale, A., Dalton, C.A., Langmuir, C., Su, Y., Schilling, J.G., 2013. The mean composition of
722 ocean ridge basalt. Geochem Geophys Geosys 14.
723 George, R., Turner, S., Hawkesworth, C.J., Morris, J., Nye, C., Ryan, J.G., Zheng, S.-H., 2003.
724 Melting processes and fluid and sediment transport rates along the Alaska-Aleutian arc
725 from an integrated U-Th-Ra-Be isotope study. J Geophys Res-Sol Ea 108, 1-25.

726 Gerya, T.V., Yuen, D.A., 2003. Rayleigh-Taylor instabilities from hydration and melting propel
727 'cold plumes' at subduction zones. Earth Planet Sc Lett 212, 47-62.
728 Grove, T., Parman, S.W., Bowring, S.A., Price, R., Baker, M.B., 2002. The role of an H_2O-rich
729 fluid component in the generation of primitive basaltic andesites and andesites from the
730 Mt. Shasta region, N California. Contrib Mineral 142, 375-396.
731 Hawkesworth, C., O'Nions, R.K., Arculus, R.J., 1979. Nd and Sr isotope geochemistry of island
732 arc volcanics, Grenada, Lesser Antilles. Earth Planet Sc Lett 45, 237-248.
733 Hawkesworth, C.J., Gallagher, K., Hergt, J.M., McDermott, F., 1993. Mantle and slab
734 contributions in arc magmas. Annual Reviews in Earth and Planetary Sciences 21, 175-
735 204.
736 Hawkesworth, C.J., Hergt, J.M., Ellam, R.M., McDermott, F., 1991. Element fluxes associated
737 with subduction related magmatism. Philosophical Transactions of the Royal Society of
738 London 335, 393-405.
739 Hawkesworth, C.J., Turner, S.P., McDermott, F., Peate, D.W., van Calsteren, P., 1997. U-Th
740 isotopes in arc magmas: Implications for element transfer from the subducted crust.
741 Science 276, 551-555.
742 Hawley, W.B., Allen, R.M., Richards, M.A., 2016. Tomography reveals buoyant asthenophere
743 accumulating beneath the Juan de Fuca plate. Science 353, 1406-1408.
744 Hermann, J., Rubatto, D., 2009. Accessory phase control on the trace element signature of
745 sediment melts in subduction zones. Chem Geol 265, 512-526.
746 Hildreth, W., Fierstein, J., 2000. Katmai volcanic cluster and the great eruption of 1912. Geol
747 Soc Am Bull 112, 1594-1620.
748 Höfig, T.W., Geldmacher, J., Hoernle, K., Hauff, F., Duggen, S., Garbe-chönberg, D., 2014.
749 From the lavas to the gabbros: 1.25 km of geochemical characterization of upper
750 oceanic crust at ODP/IODP Site 1256, eastern equatorial Pacific. Lithos 210-211, 289-
751 312.
752 Johnson, C.M., O'Neil, J.R., 1984. Triple junction magmatism: a geochemical study of Neogene
753 volcanic rocks in western California. Earth Planet Sc Lett 71, 241-262.
754 Kay, R.W., 1978. Aleutian magnesian andesites: Melts from subducted Pacific ocean crust. J
755 Volcanol Geoth Res 4, 117-132.
756 Kay, R.W., 1980. Volcanic arc magma genesis: implications for element recycling in the crust-
757 upper mantle system. Journal of Geology 88, 497-522.
758 Kay, S.M., Kay, R.W., 1994. Aleutian Magmas in Space and Time, in: Plafker, G., Berg, H.C.
759 (Eds.), The Geology of Alaska. Geological Society of America, Boulder, pp. 687-722.
760 Kelemen, P.B., Hanghøj, K., Greene, A.R., 2003a. One view of the geochemistry of subduction-
761 related magmatic arcs, with an emphasis on primitive andesite and lower crust in:
762 Holland, H.D., Turekian, K.K. (Eds.), Treatise on Geochemistry. Elsevier, New York, pp.
763 593-659.
764 Kelemen, P.B., Yogodzinski, G.M., Scholl, D.W., 2003b. Along-strike variation in lavas of the
765 Aleutian Island Arc: Implications for the genesis of high Mg# andesite and the
766 continental crust, in: Eiler, J. (Ed.), Inside the Subduction Factory, Geophysical
767 Monograph 138. American Geophysical Union, Washington D.C., pp. 223-276.
768 Kelley, K.A., Plank, T., Ludden, J.N., Staudigel, H., 2003. Composition of altered oceanic crust
769 at ODP Sites 801 and 1149. Geochem Geophys Geosys 4, 21.
770 Kessel, R., Schmidt, M.W., Ulmer, P., Pettke, T., 2005. Trace element signature of subduction-
771 zone fluids, melts and supercritical liquids at 120-180 km depth. Nature 437, 724-727.
772 Kirby, S.H., Durham, W.B., Stern, L.A., 1991. Mantle phase changes and deep-earthquake
773 faulting in subducted lithosphere. Science 252, 216-225.

774 König, S., Schuth, S., Münker, C., Qopoto, C., 2007. The role of slab melting in the petrogenesis
775 of high-Mg andesites: evidence from Simbo Volcano, Solomon Islands. Contrib Mineral
776 153, 85-103.
777 Lacasse, C., Sigurdsson, H., Carey, S.N., Jóhannesson, H., Thomas, L.E., Rogers, N.W., 2007.
778 Bimodal volcanism at the Katla subglacial caldera, Iceland: insight into the geochemistry
779 and petrogenesis of rhyolitic magmas. Bulletin of Volcanology 69, 373-399.
780 Marschall, H.R., Schumacher, J.C., 2012. Arc magmas sourced from mélange diapirs in
781 subduction zones Nature Geoscience 5, 862-867.
782 McCarron, J.J., Smellie, J.L., 1998. Tectonic implications of fore-arc magmatism and generation
783 of high-magnesian andesites: Alexander Island, Antartica. Journal of the Geological
784 Society 155, 269-280.
785 Miyashiro, A., 1974. Volcanic rock series in island arcs and active continental margins. Am J Sci
786 274, 321-355.
787 O'Neill, H.S.C., 2016. The smoothness and shapres of chondrite-normalized rare earth element
788 patterns in basalts. Journal of Petology 57, 1463-4508.
789 Peacock, S.M., 2001. Are the lower planes of double seismic zones caused by serpentine
790 dehydration in subducting oceanic mantle? Geology 29, 299-302.
791 Penniston-Dorland, S.C., Kohn, M.J., Manning, C.E., 2015. The global range of subduction zone
792 thermal structures from exhumed blueschists and eclogites: Rocks are hotter than
793 models. Earth Planet Sc Lett 428, 243-254.
794 Plank, T., 2005. Constraints from Thorium/Lanthanum on sediment recycling at subduction
795 zones and the evolution of continents. J Petrol 46, 921-944.
796 Plank, T., Cooper, L.B., Manning, C.E., 2009. Emerging geothermometers for estimating slab
797 surface temperatures. Nature Geosciences 2, 611-615.
798 Plank, T., Kelley, K.A., Zimmer, M.M., Hauri, E.H., Wallace, P.J., 2013. Why do mafic arc
799 magmas contain ~4 wt% water on average? Earth Planet Sc Lett 364, 168-179.
800 Poli, S., Schmidt, M.W., 2002. Petrology of subducted slabs. Annu Rev Earth Pl Sc 30, 207-235.
801 Portnyagin, M., Hoernle, K., Plechov, P., Mironov, N., Khubunaya, S., 2007. Constraints on
802 mantle melting and composition and nature of slab components in volcanic arcs from
803 volatiles (H2O, S, Cl, F) and trace elements in melt inclusions from the Kamchatka arc.
804 Earth Planet Sc Lett 255, 53-69.
805 Ranero, C.R., Morgan, J.P., McIntosh, K., Reichert, C., 2003. Bending-related faulting and
806 mantle serpentinization at the Middle America trench. Nature 425, 367-373.
807 Rogers, G., Saunders, A.D., Terrell, D.J., Verma, S.P., Marriner, G.F., 1985. Geochemistry of
808 Holocene volcanic rocks associated with ridge subduction in Baja, California, Mexico.
809 Nature 315, 389-392.
810 Salters, V.J.M., Stracke, A., 2003. Composition of the depleted mantle. Geochemistry,
811 Geophysics, Geosystems 5, doi:10.1029/2003GC000597.
812 Scambelluri, M., Fiebig, J., Malaspina, N., Müntener, O., Pettke, T., 2004. Serpentinite
813 subduction: Implications for fluid processes and trace-element recycling International
814 Geology Review 46, 595-613.
815 Schmidt, M.W., Vielzeuf, D., Auzanneau, E., 2004. Melting and dissolution of subducting crust at
816 high pressures: the key role of white mica. Earth Planet Sc Lett 228, 65-84.
817 Sisson, T.W., Grove, T.L., 1993. Experimental investigations of the role of H_2O in calc-alkaline
818 differentiation and subduction zone magmatism. Contrib Mineral 113, 143-166.
819 Skora, S., Blundy, J., 2010. High-pressure hydrous phase relatinos of radiolarian clay and
820 implications for the involvement of subducted sediment in arc magmatism. Journal of
821 Petology 51, 2211-2243.

822 Spandler, C., Pettke, T., Hermann, J., 2014. Experimental study of trace element release during
823 ultrahigh-pressure serpentinite dyhydration. Earth Planet Sc Lett 391, 296-306.
824 Staudigel, H., 2003. Hydrothermal Alertation Processes in the Oceanic Crust, in: Turekian, K.K.,
825 Holland, H.D. (Eds.), The Crust: Treatise on Geochemistry v. 3. Elsevier, Newnes, pp.
826 511-535.
827 Stern, C.R., Killian, R., 1996. Role of the subducted slab, mantle wedge and continental crust in
828 the generation of adakites from the Andean Austral Volcanic Zone. Contrib Mineral 123,
829 263-281.
830 Syracuse, E.M., Abers, G.A., 2006. Global compilation of variations in slab depth beneath arc
831 volcanoes and implications. Geochem Geophys Geosys 7, Q05017,
832 doi:05010.01029/02005GC001045.
833 Syracuse, E.M., van Keken, P.E., Abers, G.A., 2010. The global range of subduction zone
834 thermal models. Phys Earth Planet In 183, 73-90.
835 Tamura, Y., Gill, J.B., Tollstrup, D., Kawabata, H., Shkuno, H., Chang, Q., Miyazaki, T.,
836 Takahashi, N., Hirahara, Y., Kodaira, S., Ishizuka, O., Suzuki, T., Kido, Y., Fiske, R.S.,
837 Tatsumi, Y., 2009. Silicic magmas in the Izu-Bonin oceanic arc and implicatins for crustal
838 evolution. J Petrol 50, 685-723.
839 Tatsumi, Y., Hamilton, D.L., Nesbitt, R.W., 1986. Chemical characteristics of fluid phase
840 released from a subducted lithosphere and origin of arc magmas: evidence from high-
841 pressure experiments and natural rocks. J Volcanol Geoth Res 29, 293-309.
842 Taylor, H.P., Sheppard, S.M.F., 1986. Igneous Rocks; I, Processes of isotopic fractionation and
843 isotope systematics. Reviews in Mineralogy and Geochemistry 16, 227-271.
844 Tenthorey, E., Hermann, J., 2004. Composition of fluids during serpentinite breakdown in
845 subduction zones: evidence for limited boron mobility. Geology 32, 865-868.
846 Tollan, P.M.E., Bindeman, I., Blundy, J., 2012. Cumulate xenoliths from St. Vincent, Lesser
847 Antilles Island Arc: a window into upper crustal differentiation of mantle-derived basalts.
848 Contrib Mineral 163, 189-208.
849 Turner, S., Hawkewsworth, C., van Calsteren, P., Heath, E., Macdonald, R., Black, S., 1996. U-
850 series isotopes and destructive plate margin magma genesis in the Lesser Antilles.
851 Earth Planet Sc Lett 142, 191-207.
852 Ulmer, P., Trommsdorff, V., 1995. Serpentine stability to mantle depths and subduction-related
853 magmatism. Science 268, 858-861.
854 van Keken, P.E., Hacker, B.R., Syracuse, E.M., Abers, G.A., 2011. Subduction factory: 4.
855 Depth-dependent flux of H2O from subducting slabs worldwide. J Geophys Res-Sol Ea
856 116.
857 Walowski, K.J., Wallace, P.J., Hauri, E.H., Wada, I., Clynne, M.A., 2015. Slab melting beneath
858 the Cascade Arc driven by dehydration of altered oceanic peridotite. Nature
859 Geosciences 8, 404-408.
860 Wanless, V.D., Perfit, M.R., Ridley, W.I., Klein, E., 2010. Dacite petrogenesis on mid-ocean
861 ridges: Evidence for oceanic crustal melting and assimilation. Journal of Petology 51,
862 2377-2410.
863 Yamaoka, K., Fukao, Y., Kumazawa, M., 1986. Spherical shell tectonics: Effects of sphericity
864 and inextensibility on the geometry of the descending lithosphere. Rev Geophys 24, 27-
865 53.
866 Yogodzinski, G.M., Brown, S.T., Kelemen, P.B., Vervoort, J.D., Portnyagin, M., Sims, K.W.W.,
867 Hoernle, K., Jicha, B., Werner, R., 2015. The role of subducted basalt in the source of
868 island arc magmas: evidence from seafloor lavas of the western Aleutians. J Petrol 56,
869 441-492.

Yogodzinski, G.M., Kay, R.W., Volynets, O.N., Koloskov, A.V., Kay, S.M., 1995. Magnesian andesite in the western Aleutian Komandorsky region: Implications for slab melting and processes in the mantle wedge. Geol Soc Am Bull 107, 505-519.

Yogodzinski, G.M., Kelemen, P.B., 1998. Slab melting in the Aleutians: implications of an ion probe study of clinopyroxene in primitive adakite and basalt. Earth Planet Sc Lett 158, 53-65.

Yogodzinski, G.M., Lees, J.M., Churikova, T.G., Dorendorf, F., Wörner, G., Volynets, O.N., 2001. Geochemical evidence for the melting of subducting oceanic lithosphere at plate edges. Nature 409, 500-504.

Yogodzinski, G.M., Volynets, O.N., Koloskov, A.V., Seliverstov, N.I., Matvenkov, V.V., 1994. Magnesian andesites and the subduction component in a strongly calc-alkaline series at Piip Volcano, far western Aleutians. J Petrol 35, 163-204.

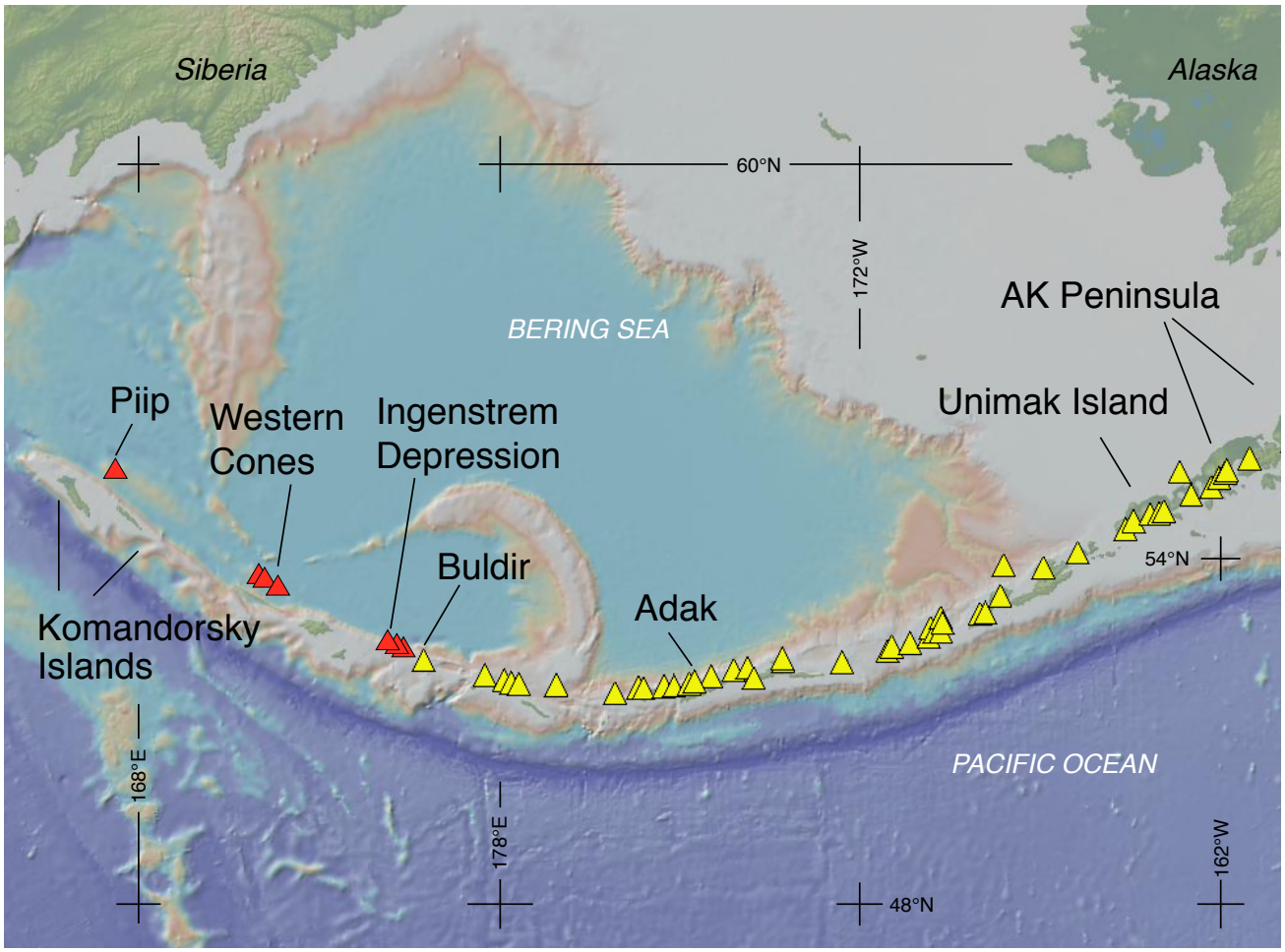
Siberia
Alaska
60°N
172°W
BERING SEA
AK Peninsula
Unimak Island
Piip
Western
Cones
Ingenstrem
Depression
Buldir
Adak
54°N
Komandorsky
Islands
168°E
178°E
PACIFIC OCEAN
48°N
162°W

Fig. 1

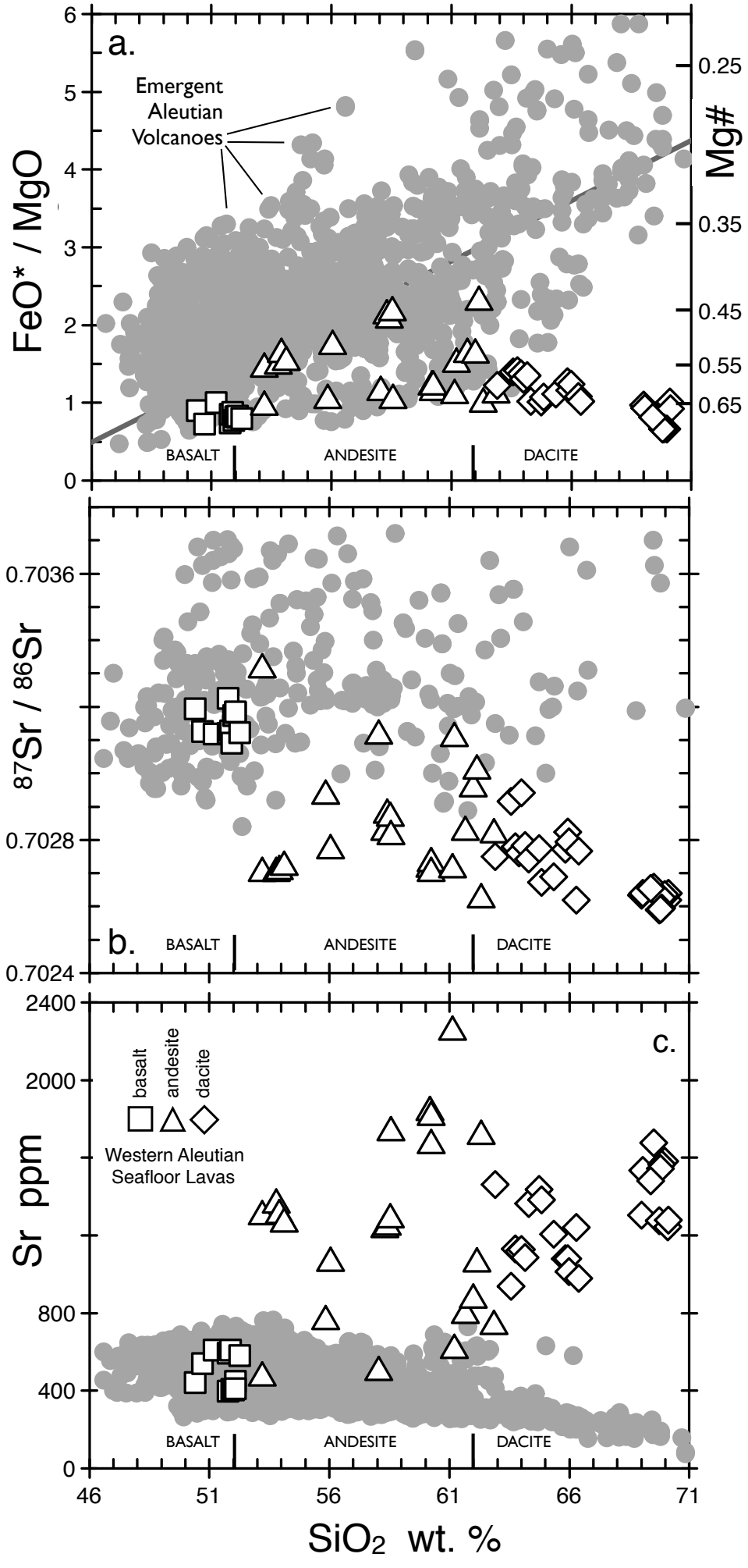
a.
Emergent
Aleutian
Volcanoes
FeO* / MgO
Mg#
0.25
0.35
0.45
0.55
0.65
BASALT
ANDESITE
DACITE
0.7036
0.7028
0.7024
^{87}Sr / ^{86}Sr
b.
2400
2000
800
400
0
Sr ppm
c.
basalt
andesite
dacite
Western Aleutian
Seafloor Lavas
46
51
56
61
66
71
SiO_2 wt. %

Fig. 2

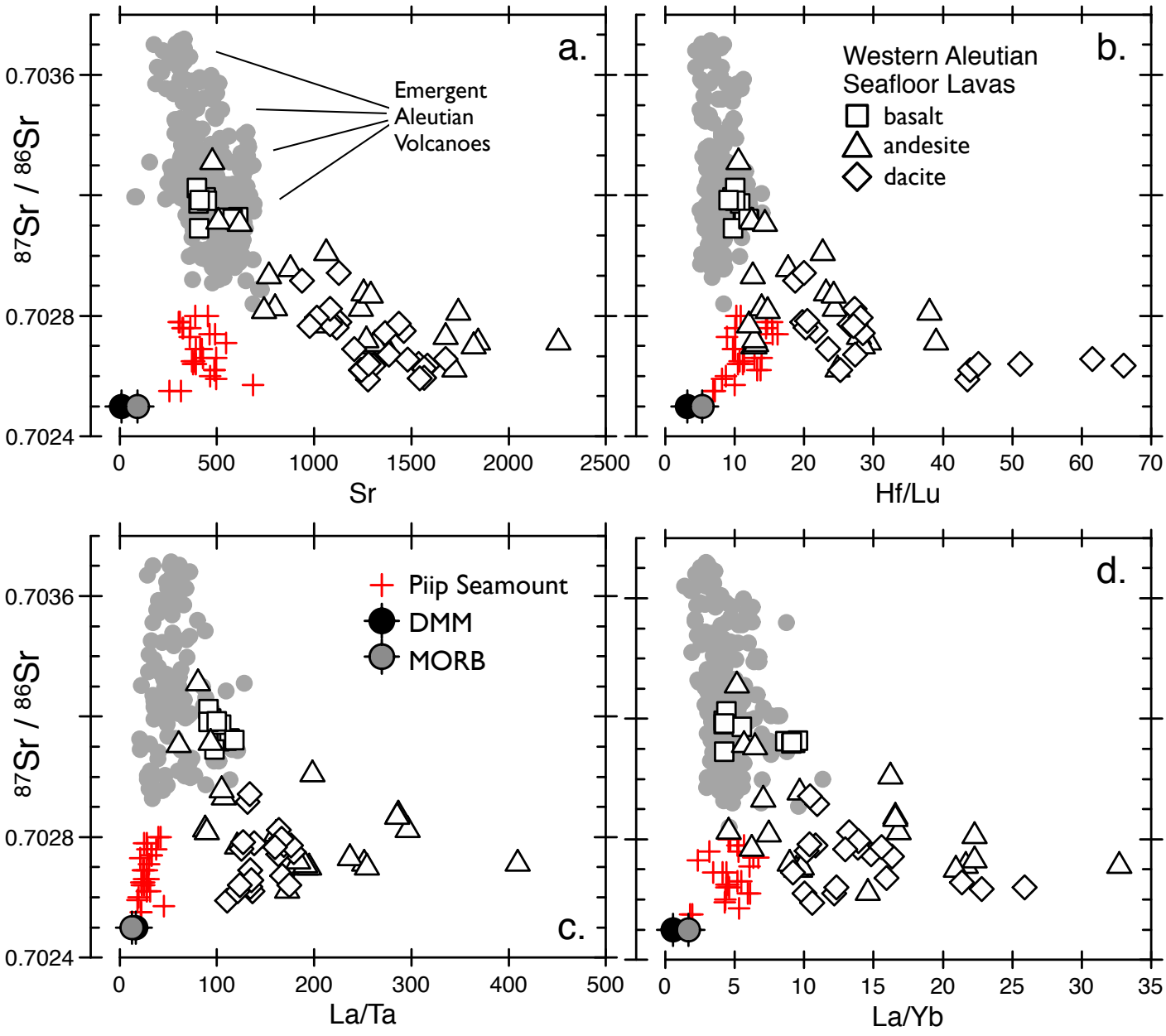
a.
b.
c.
d.
Emergent
Aleutian
Volcanoes
Western Aleutian
Seafloor Lavas
basalt
andesite
dacite
Piip Seamount
DMM
MORB
87Sr / 86Sr
0.7036
0.7028
0.7024
Sr
Hf/Lu
La/Ta
La/Yb
0
500
1000
1500
2000
2500
10
20
30
40
50
60
70
100
200
300
400
5
15
25
35

Fig. 3

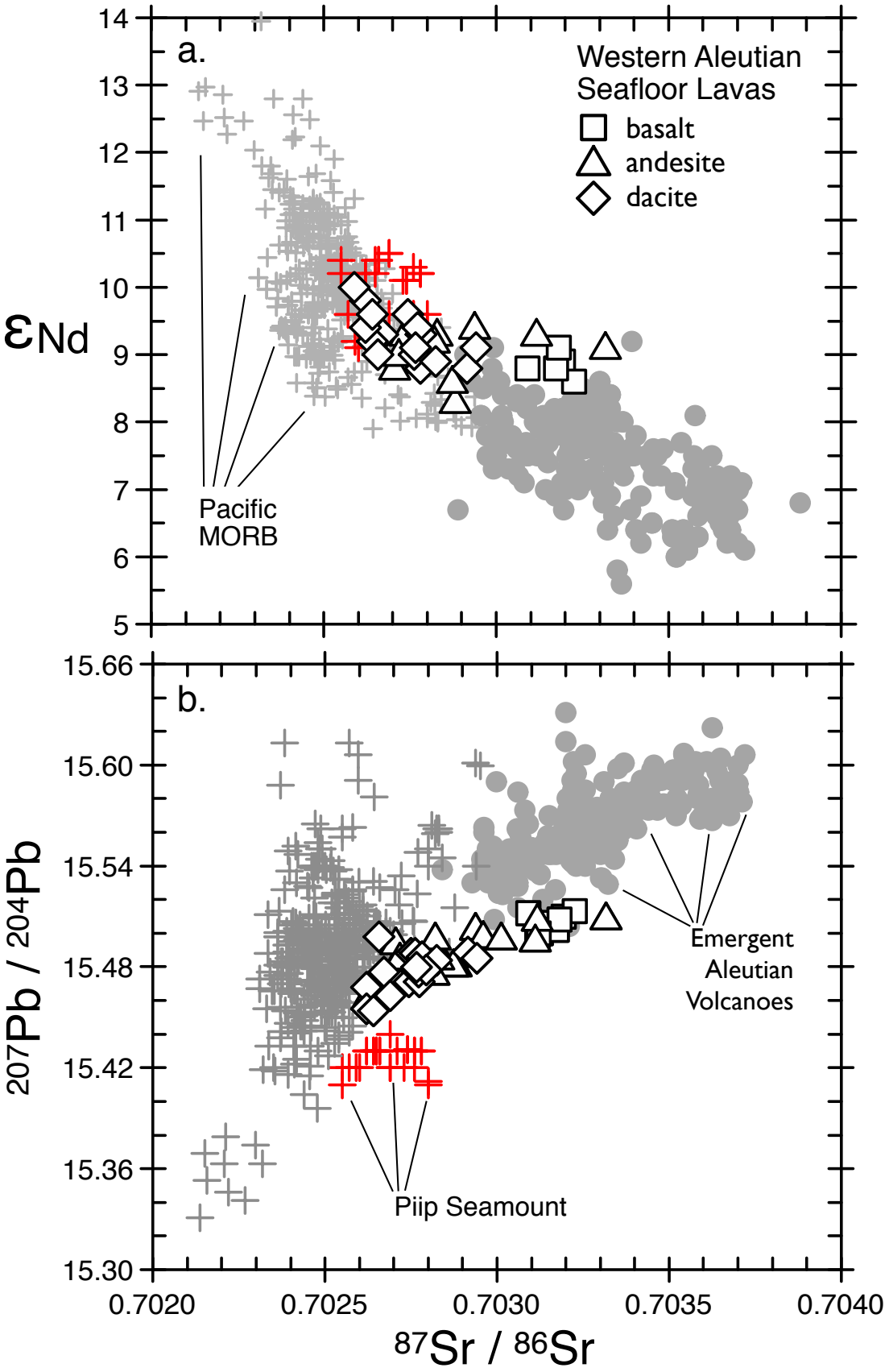
a.
Western Aleutian
Seafloor Lavas
basalt
andesite
dacite
εNd
Pacific
MORB
b.
Emergent
Aleutian
Volcanoes
Piip Seamount
207Pb / 204Pb
87Sr / 86Sr
14
13
12
11
10
9
8
7
6
5
15.66
15.60
15.54
15.48
15.42
15.36
15.30
0.7020
0.7025
0.7030
0.7035
0.7040

Fig. 4

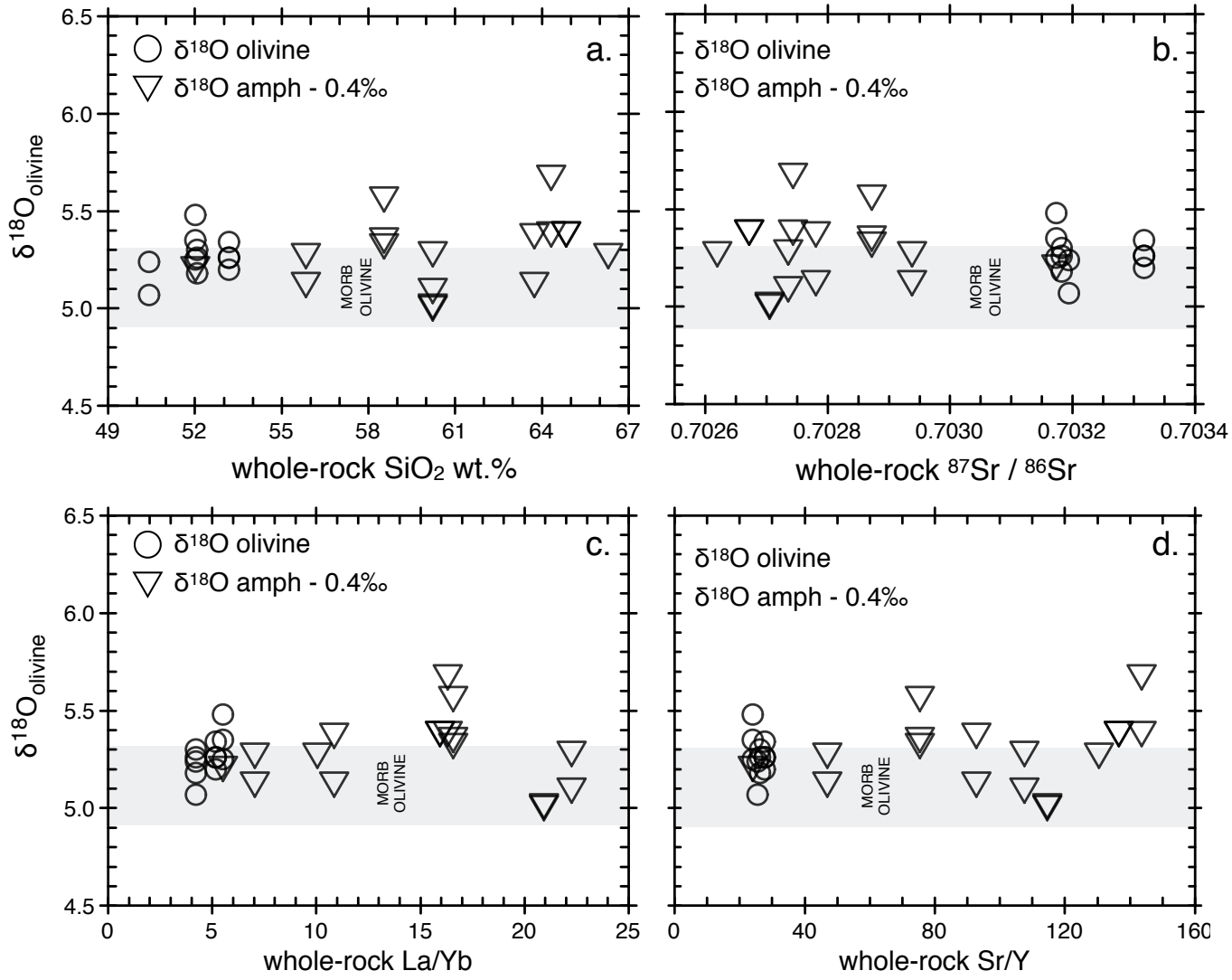
a.
b.
c.
d.
δ18O olivine
δ18O amph - 0.4‰
MORB OLIVINE
δ18Oolivine
whole-rock SiO2 wt.%
whole-rock 87Sr / 86Sr
whole-rock La/Yb
whole-rock Sr/Y
6.5
6.0
5.5
5.0
4.5
49
52
55
58
61
64
67
0.7026
0.7028
0.7030
0.7032
0.7034
0
5
10
15
20
25
40
80
120
160

Fig. 5

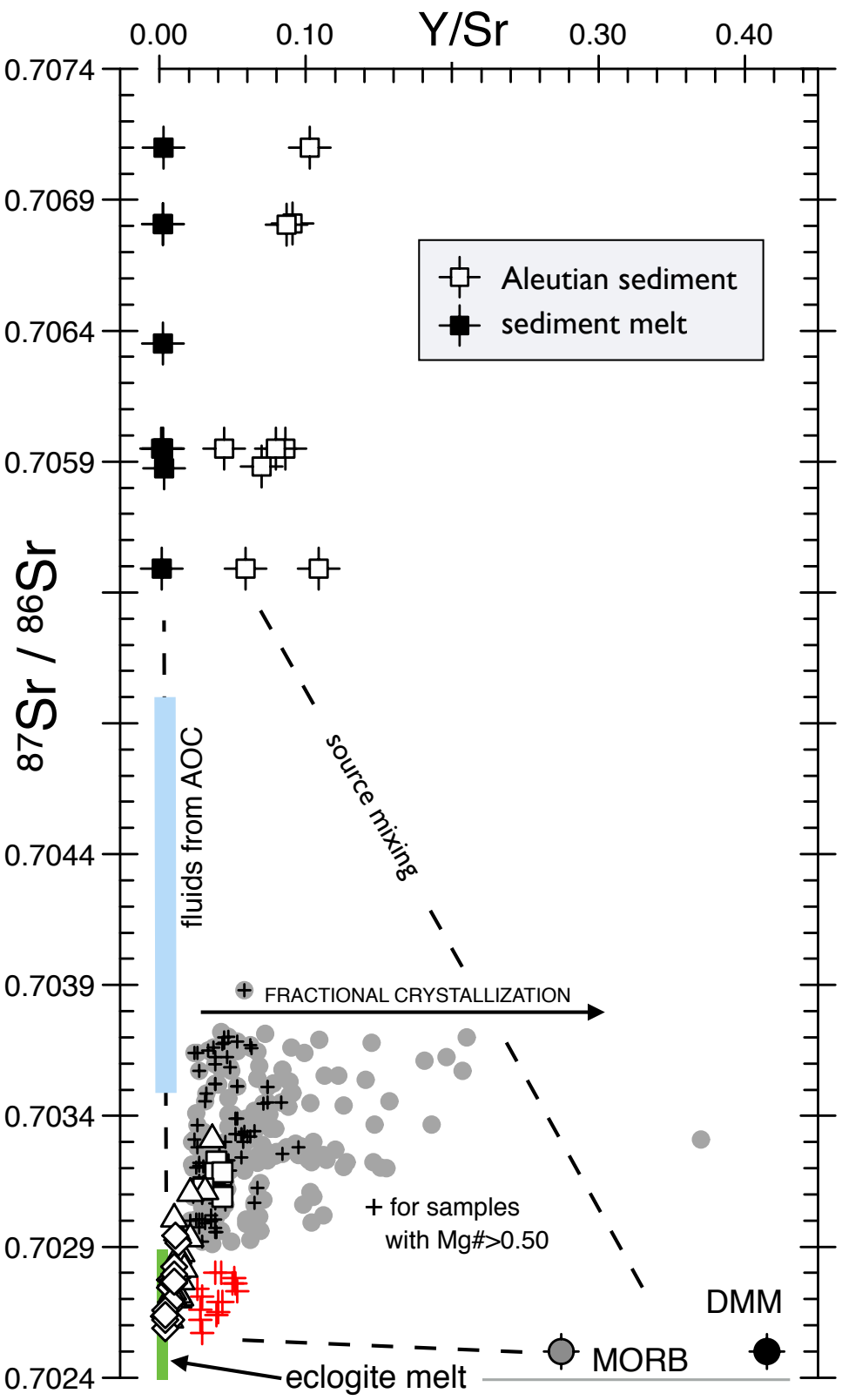
Y/Sr
0.00
0.10
0.30
0.40
0.7074
0.7069
0.7064
0.7059
0.7044
0.7039
0.7034
0.7029
0.7024
87Sr / 86Sr
Aleutian sediment
sediment melt
fluids from AOC
source mixing
FRACTIONAL CRYSTALLIZATION
+ for samples
with Mg#>0.50
DMM
MORB
eclogite melt

Fig. 6

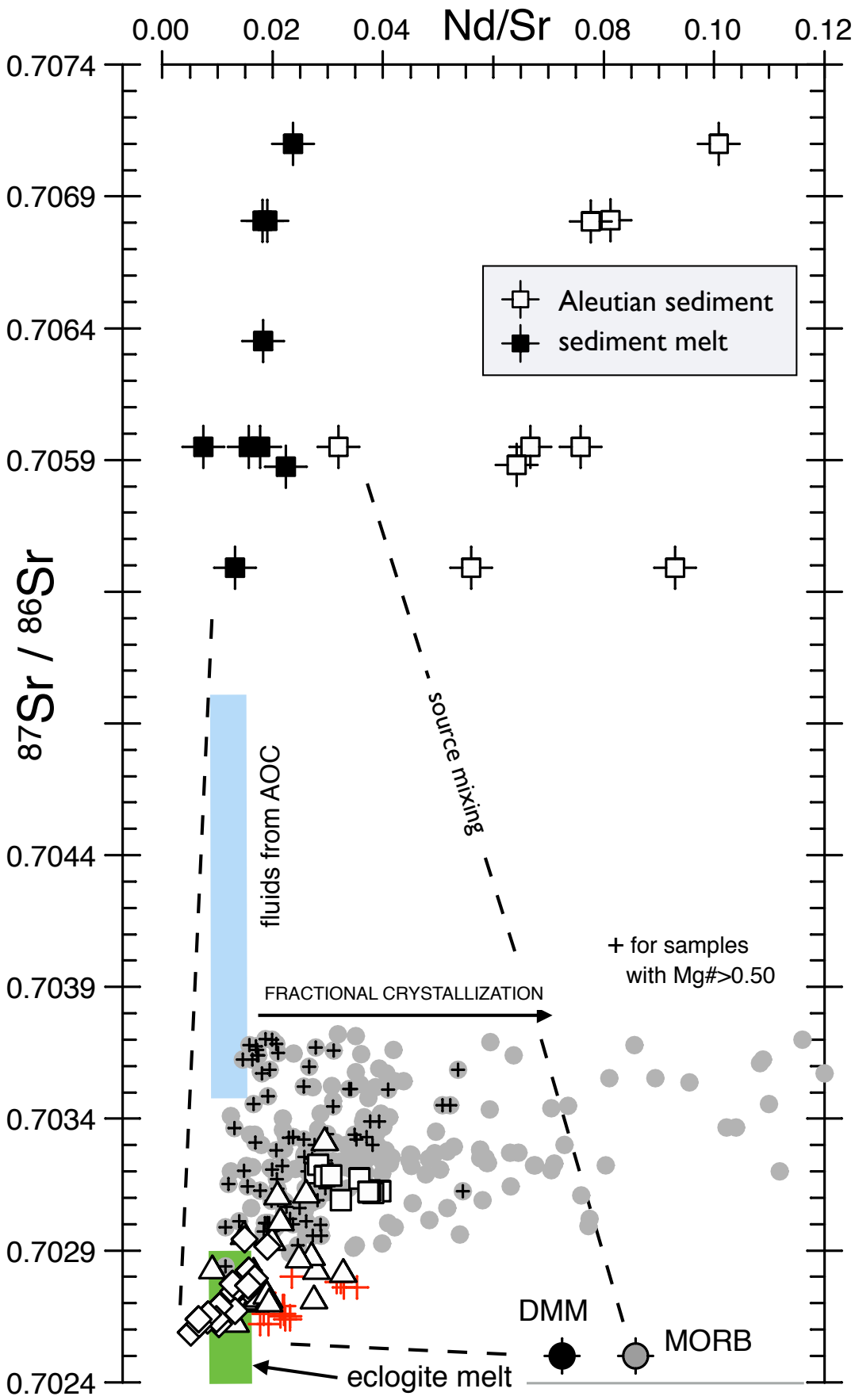
Nd/Sr
0.00
0.02
0.04
0.08
0.10
0.12
0.7074
0.7069
0.7064
0.7059
0.7044
0.7039
0.7034
0.7029
0.7024
87Sr / 86Sr
Aleutian sediment
sediment melt
fluids from AOC
source mixing
+ for samples
with Mg#>0.50
FRACTIONAL CRYSTALLIZATION
DMM
MORB
eclogite melt

Fig. 7

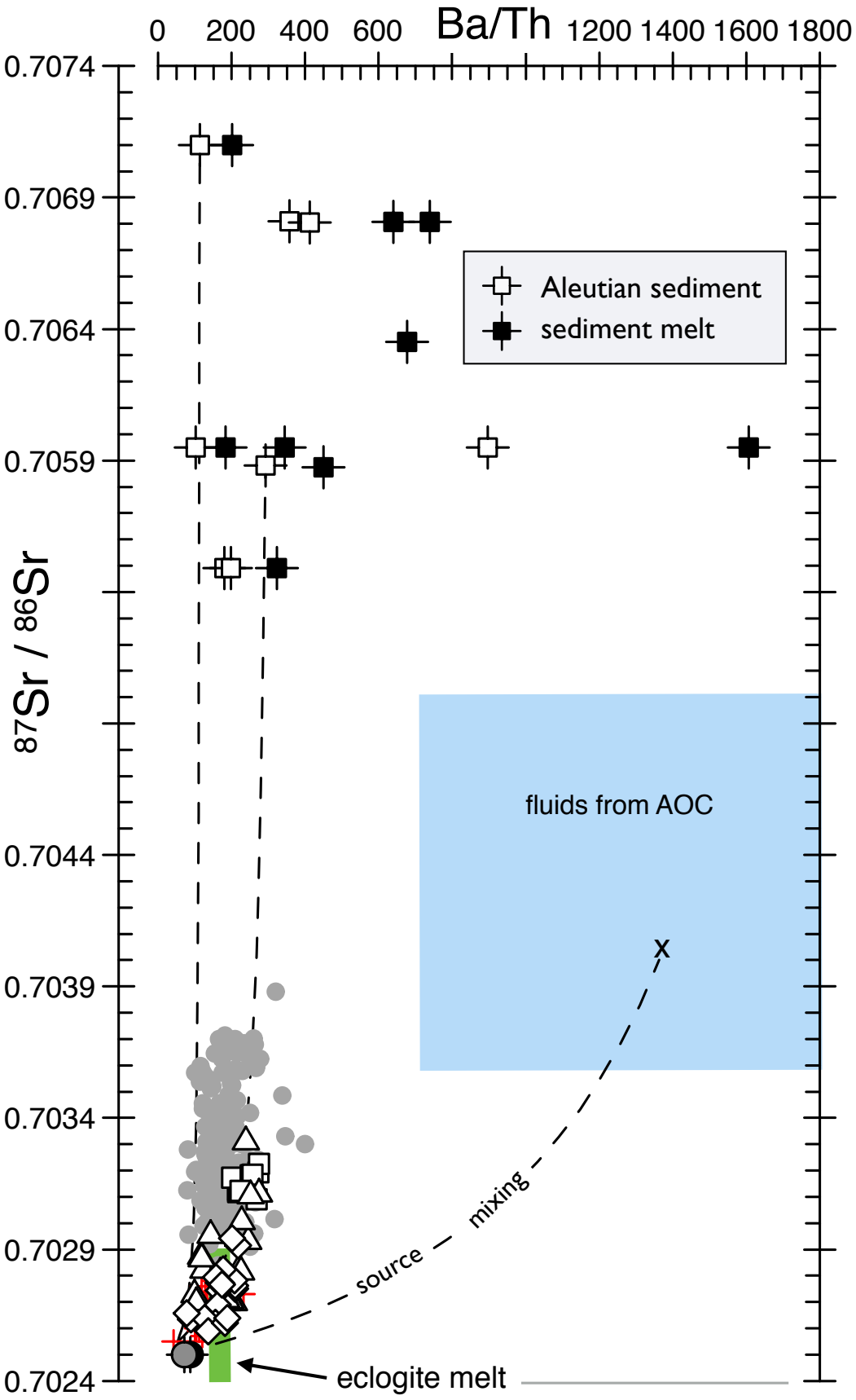
Ba/Th
0
200
400
600
1200
1400
1600
1800
0.7074
0.7069
0.7064
0.7059
0.7044
0.7039
0.7034
0.7029
0.7024
87Sr / 86Sr
Aleutian sediment
sediment melt
fluids from AOC
x
source
mixing
eclogite melt

Fig. 8

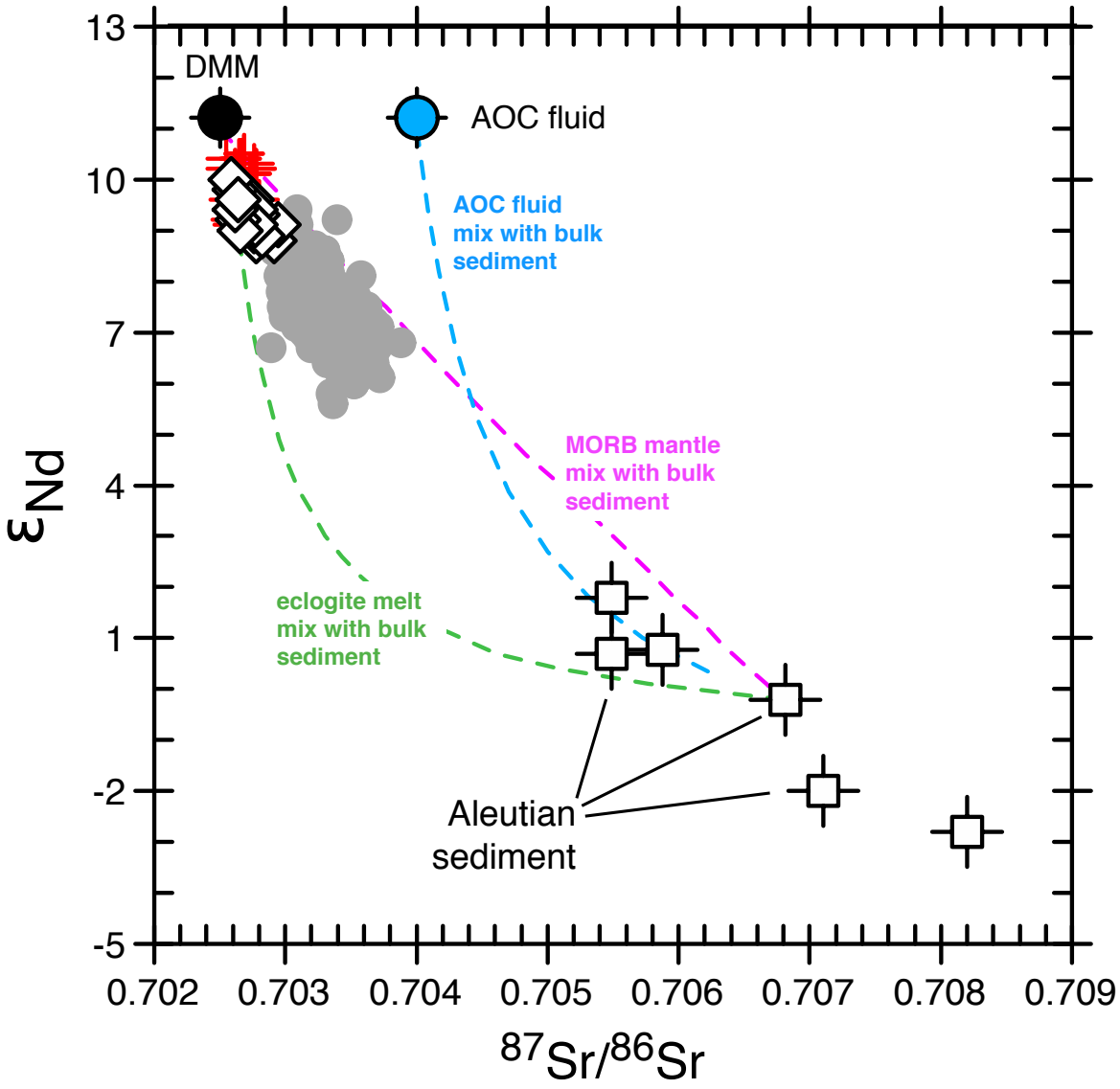
13
10
7
4
1
-2
-5
εNd
0.702
0.703
0.704
0.705
0.706
0.707
0.708
0.709
87Sr/86Sr
DMM
AOC fluid
AOC fluid
mix with bulk
sediment
MORB mantle
mix with bulk
sediment
eclogite melt
mix with bulk
sediment
Aleutian
sediment

Fig. 9

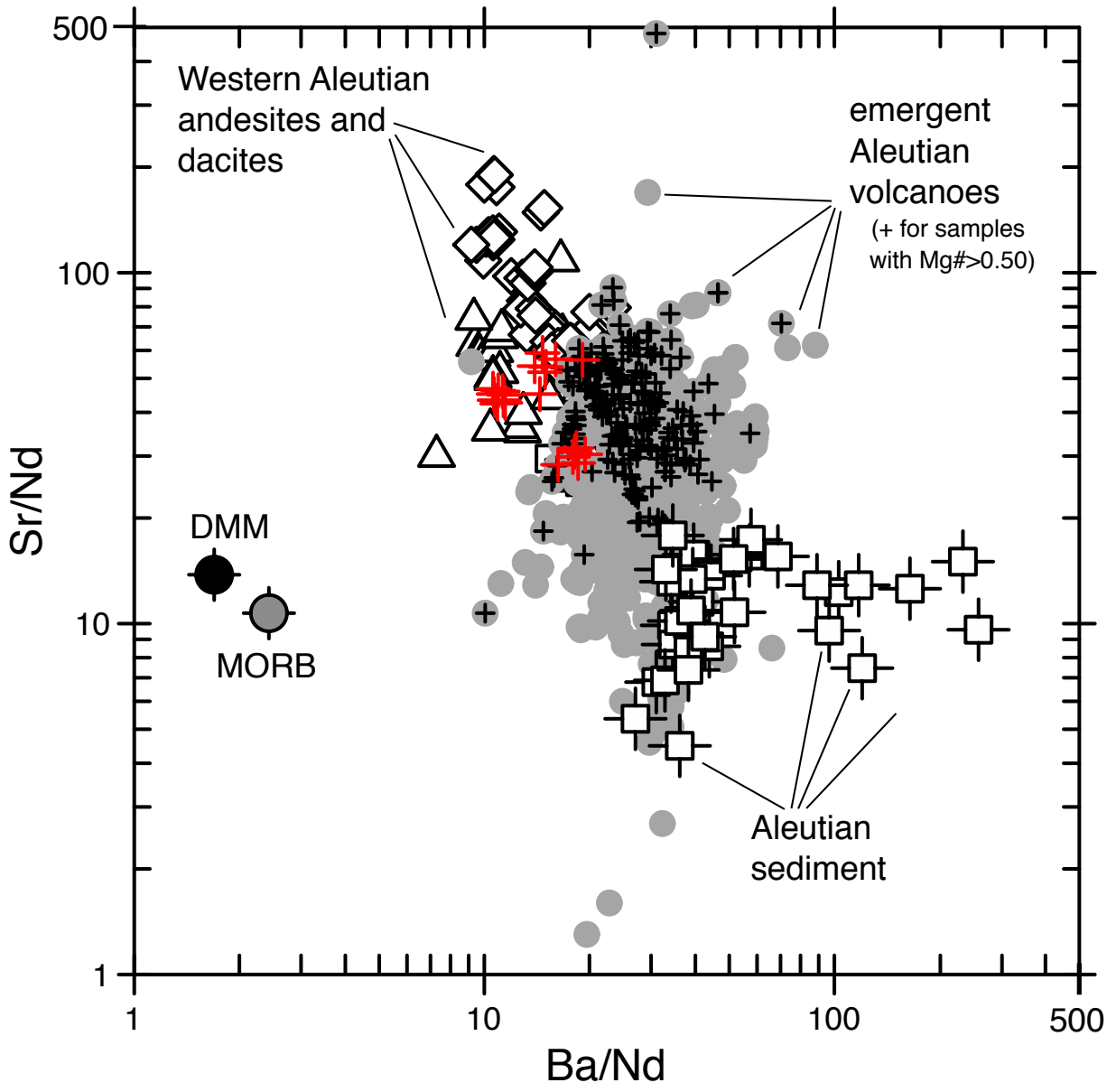
500
100
10
1
Sr/Nd
1
10
100
500
Ba/Nd
Western Aleutian
andesites and
dacites
emergent
Aleutian
volcanoes
(+ for samples
with Mg#>0.50)
DMM
MORB
Aleutian
sediment

Fig. 10